TRIUMF

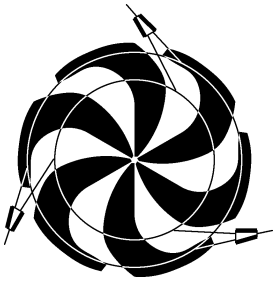

ANNUAL REPORT
SCIENTIFIC ACTIVITIES
2001

ISSN 1492-417X

CANADA'S NATIONAL LABORATORY
FOR PARTICLE AND NUCLEAR PHYSICS

OPERATED AS A JOINT VENTURE

MEMBERS:

THE UNIVERSITY OF ALBERTA
THE UNIVERSITY OF BRITISH COLUMBIA
CARLETON UNIVERSITY
SIMON FRASER UNIVERSITY
THE UNIVERSITY OF VICTORIA

ASSOCIATE MEMBERS:

THE UNIVERSITY OF MANITOBA
McMASTER UNIVERSITY
L'UNIVERSITÉ DE MONTRÉAL
QUEEN'S UNIVERSITY
THE UNIVERSITY OF REGINA
THE UNIVERSITY OF TORONTO

UNDER A CONTRIBUTION FROM THE
NATIONAL RESEARCH COUNCIL OF CANADA

OCTOBER 2002

The contributions on individual experiments in this report are outlines intended to demonstrate the extent of scientific activity at TRIUMF during the past year. The outlines are not publications and often contain preliminary results not intended, or not yet ready, for publication. Material from these reports should not be reproduced or quoted without permission from the authors.

Experiment 758
Effects of quantum impurities in graphite and in one dimensional spin 1/2 chain CPC
(R.F. Kiefl, UBC/TRIUMF; J. Chakhalian, UBC)

Graphite

The purpose of these experiments is to test theoretical predictions on the effects of quantum impurities. The electronic and magnetic properties of an isolated positively charged impurity in a degenerate electron gas have been the subject of numerous theoretical studies [van Dyke, Nucl. Mater. **67-70**, 533 (1978); Lane and Cloney, *ibid.*, 582; Popovic and Scott, Phys. Rev. **B5**, 2109 (1972); Zaremba *et al.*, J. Physics **F7**, 1763 (1977); Jena and Singwi, Phys. Rev. **B17**, 3518 (1978)] because of its fundamental importance. Interesting quantum critical phenomena occur when gapless bulk magnetic excitations interact with a single charge impurity. The most well-known example is the Kondo effect in normal metals where a particularly large modification of the local susceptibility in the vicinity of the impurity occurs at low T.

In order to verify the theories, we have studied the local electronic structure for muons implanted in HOPG graphite by means of the muon Knight shift measurements from 3 K to 900 K. The measured Knight shift in graphite is unusually large and temperature dependent which indicates the formation of a local moment (see Fig. 58).

This is in contrast to normal metals where the Knight shifts are small and scale with the Pauli susceptibility. The isotropic part of the Knight shift is much larger than the dipolar part and rises with temperature as shown in Fig. 59. We have interpreted these results in terms of a local model where the spin density is predominantly on the neighbouring carbons, which is similar to what is observed in some semiconductors (e.g. GaAs). This is also consistent with recent molecular orbital calculation for hydrogen on a single graphite sheet [Cox *et al.*, J. Phys. Cond. Matter **13**, 2169 (2001)].

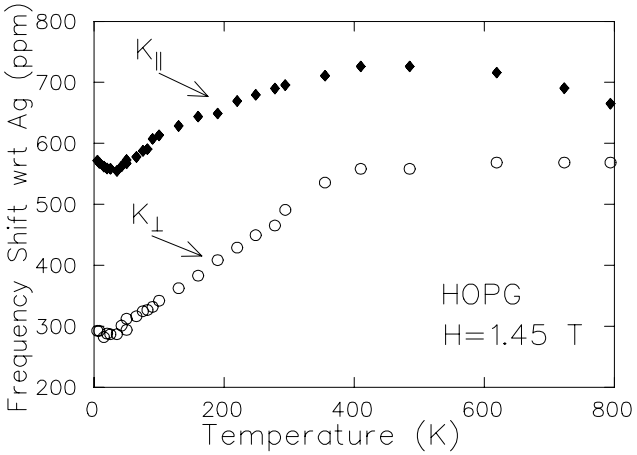

Fig. 58. Shift in muon precession frequency in HOPG relative to Ag as a function of temperature in an applied magnetic field of 1.45 T.

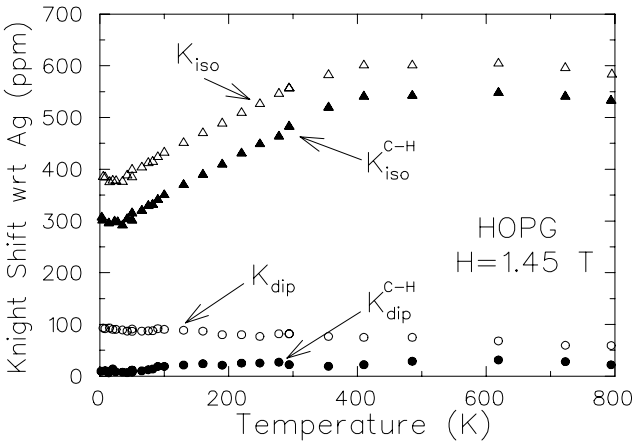

Fig. 59. Temperature dependence of the isotropic $\mathcal{K}_{\rm iso}$ and axial or dipolar $\mathcal{K}_{\rm dip}$ parts of the muon Knight shift in graphite. The filled circles and triangles represent the corrected value of the Knight shift assuming that a muon is at the C-H bond distance from a carbon atom. The open circles and triangles represent the corrected Knight shift assuming that μ^+ is in the interplane position.

The increase in the isotropic part of the Knight shift, which measures the contact interaction, indicates that the local electronic structure changes with temperature. At very low temperatures the observed upturn in $\mathcal{K}_{\|}$ is attributed to the bulk susceptibility, which is influenced by the De Haas–van Alphen effect at low T.

In addition, the measured muon spin relaxation rate $1/T_1$ is unusually large and deviates from the Korringa relation for metals (see Fig. 60).

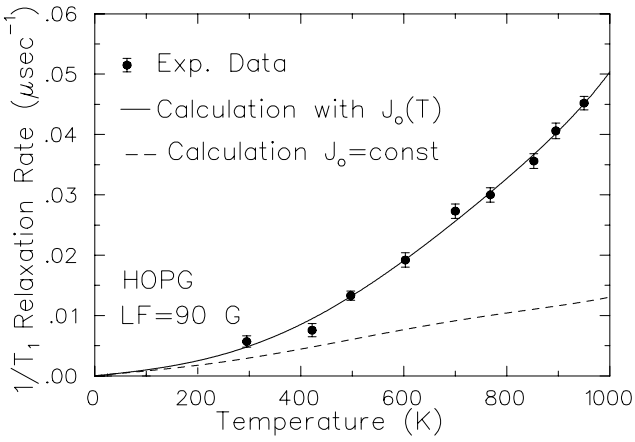

Fig. 60. Temperature dependence of the longitudinal relaxation rate $1/T_1$ in pure graphite measured above RT. The solid and dashed lines represent our estimates.

This is attributed in part to a strong energy dependence in the density of states coupled with a small Fermi energy. A phenomenological model based on the specific graphite density of states and the temperature dependent coupling constant $J(T)$ describes the $1/T_1$ data rather well (see solid line in Fig. 60). The large extracted value of the Kondo temperature, $T_K =$ 1852(40) K, is consistent with the strong-coupling limit picture. It is also worth noting that the conventional Kondo problem has only been extensively studied for normal metals where k_BT is much less than E_F, i.e. the degenerate electron gas. The situation in graphite is quite different: there, E_F is comparable to k_BT.

CPC

Recent theoretical work by Affleck, Eggert and Takashi (AET) indicates interesting behaviour in an s=l/2 Heisenberg anti-ferromagnetic spin chain with a non-magnetic single impurity [Eggert and Affleck, Phys. Rev. **B46**, 10866 (1992); Affleck *et al.*, J. Phys. **A22**, 511 (1989); Eggert and Affleck, Phys. Rev. Lett. **75**, 934 (1995)]. This behaviour is attributed to the gapless spectrum of magnetic excitations and may be considered the magnetic equivalent of the Kondo effect in normal metals. Weakening a single link in the chain as shown in Fig. 61 is a relevant perturbation; the system behaves at low T as if the chain was severed. In contrast, there is considerable experimental evidence that in most two and three dimensional magnetic compounds the muon impurity has a negligible effect, i.e. the local magnetic susceptibility tracks the bulk susceptibility.

As expected from the theory, any generic perturbation (which is not site-parity symmetric) is relevant and should result in a renormalization to a completely broken chain.

To test the theory, we conducted the μSR measurements on the quasi one dimensional s=1/2 antiferromagnetic insulating chain – dichlorobis (pyridine)

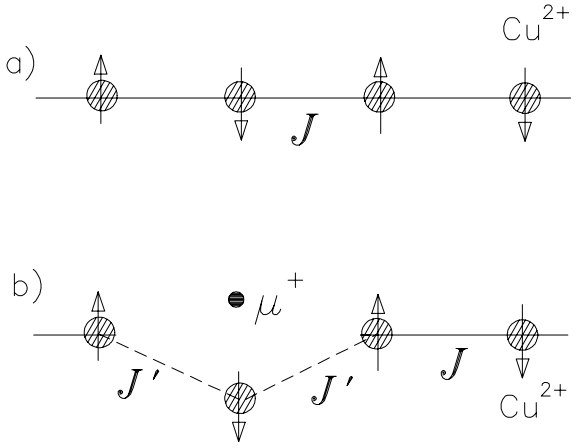

Fig. 61. A quantum spin chain with one altered link. A possible position of the muon is indicated by the arrow.

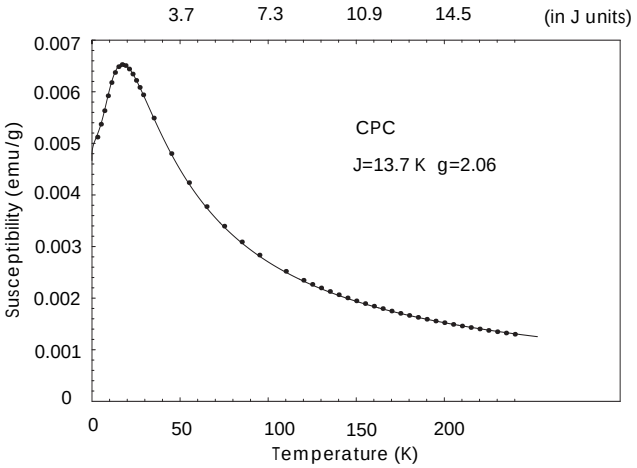

Fig. 62. Theoretical quantum Monte Carlo fit to the SQUID CPC data: The data were taken in an applied magnetic field of 1.45 T. The fit is provided courtesy of S. Eggert.

copper(II) (CPC). The AET theory predicts that the local magnetic susceptibility near an impurity in a spin 1/2 chain is dramatically different compared to the bulk magnetic susceptibility. To verify the AET theory, we compared the local spin susceptibility as measured by the muon spin precession frequency with the bulk magnetic susceptibility measured in a SQUID magnetometer. The theoretical fit to the experimental unperturbed susceptibility data is excellent over the entire temperature range (see Fig. 62).

The best fit yields a value of the intrachain coupling constant of $J = 13.7(1)$ K and a g-factor of 2.06(1). This estimate of J is about 2% larger than previously reported [Takeda *et al.*, J. Phys. Soc. Japan **30**, 1330 (1971)].

In CPC the measured muon frequency shift shows a dramatic difference between the local and bulk magnetic response. The fast Fourier transforms display complex multiple frequency spectra present at low temperatures below 30 K (see Fig. 63).

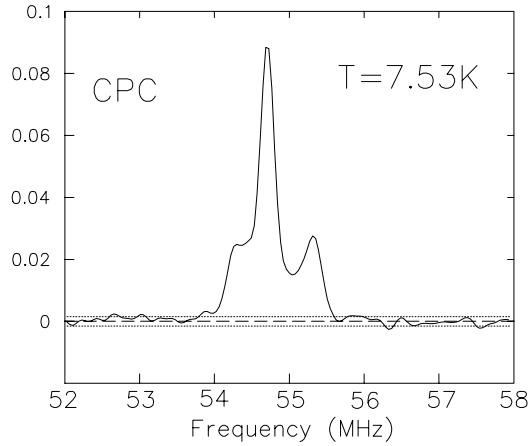

Fig. 63. FFT transform of the μSR signal at 7.53 K.

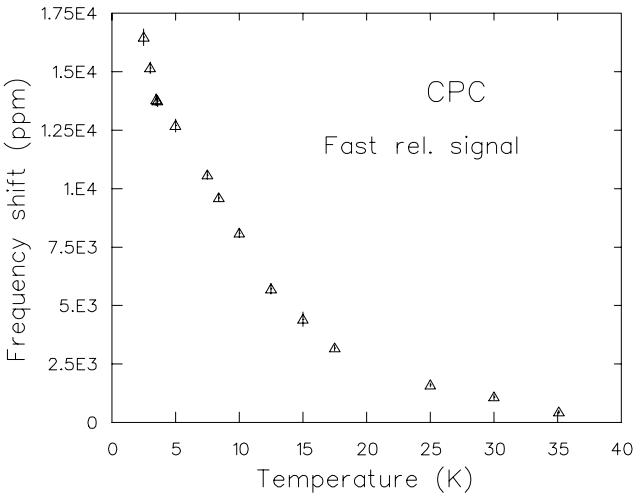

Fig. 64. Frequency shift of one of the fast relaxing μSR signals in CPC.

This probably represents localization of the muon at magnetically inequivalent sites. The characteristic maximum around 18 K seen in the unperturbed d.c. susceptibility is completely washed out in the frequency shift of the fast relaxing signals (see Fig. 64), which is clear evidence for a strong perturbation and thus supports the validity of the AET theory.

Experiment 775
Electron transport in insulators, semiconductors and magnetic materials
(J.H. Brewer, UBC; G.M. Luke, Columbia; V. Storchak, Kurchatov)

Influence of impurities on short range electron transport in GaAs

The electronic structure and dynamics of isolated atomic hydrogen (H) in semiconductors is of fundamental interest since it is the simplest and the lightest interstitial impurity. Unfortunately, direct information on isolated hydrogen is extremely limited due to its high mobility and reactivity. Most of the experimental information on the interstitial hydrogen atom comes indirectly from studies of the muonium ($\mathrm{Mu} = \mu^+ e^-$) atom. However, one should always keep in mind that hydrogen and muonium are incorporated into a semiconductor in two very different ways. Hydrogen is introduced during the process of sample preparation and reaches thermal and chemical equilibrium before measurements start, while muonium is observed starting a few nanoseconds after the injection of energetic (about 4 MeV) muons into the sample [Schenck, Muon Spin Rotation: Principles and Applications in Solid State Physics (Adam Hilger, Bristol, 1986); Cox, J. Phys. **C20**, 3187 (1987); Brewer, *Muon spin rotation-relaxation-resonance* in Encyclopedia of Applied Physics (VCH Publishers, New York, 1994) **11**, 23]. As the energetic μ^+ slows to an energy of a few tens of keV, in insulators and semiconductors the positive muon undergoes many cycles of electron capture and subsequent electron loss. If the last such collision leaves atomic Mu in its neutral charge state, muonium is said to have been formed promptly. If the μ^+ thermalizes as a positive ion, in many materials some of the excess electrons generated in its ionization track can reach the stopped muon and form muonium. This process of "delayed" muonium formation (DMF) is crucially dependent on the electron's interaction with its environment or the electron mobility. Note that the characteristic length-scale of DMF is essentially microscopic – less than 10^{-4} cm [Storchak *et al.*, Appl. Mag. Reson. **13**, 15 (1997)]. This fact offers a unique opportunity for study of electron transport to positive centres on a microscopic scale.

An essential feature of DMF is that the electrons start out spatially separated from the muon; this property is the key to distinguishing experimentally between delayed and prompt Mu formation by applying external electric fields [Storchak *et al.*, Phys. Rev. Lett. **75**, 2384 (1995); Eshchenko, Ph.D. thesis (Kurchatov Institute, Moscow, 1996) (in Russian)]. Relatively weak external electric fields ($\sim 10^4$ V/cm) can sometimes overcome the muon-electron Coulomb attraction and thus reduce the probability of DMF, whereas electric fields of atomic strength ($\sim 10^8 - 10^9$ V/cm) would be required to affect prompt (epithermal) Mu formation.

In most semiconductors two quite different types of muonium centres coexist with the diamagnetic state (or states) of the muon [Patterson, Rev. Mod. Phys. **60**, 69 (1988); Estle and Lichti, Hyp. Int. **97-98**, 171 (1996); Kiefl *et al.*, Phys. Rev. Lett. **58**, 1780 (1987)]. So-called "normal" muonium has an isotropic hyperfine interaction with a hyperfine constant of about half the free muonium value and is located at the tetrahedral interstitial site (and is thus denoted as Mu_T^0). "Anomalous" or "bond-centred" muonium, with a small anisotropic hyperfine interaction, is located near the centre of the relaxed crystal bond (and is thus denoted as Mu_{BC}^0).

Recent experiments with semi-insulating GaAs [Eshchenko *et al.*, Phys. Lett. **A264**, 226 (1999)] have shown complete suppression of the Mu_{BC}^0 signal with electric field. This fact is illustrated in Fig. 65. One can see a large multi-frequency muonium signal for $E = 0$; this beating is absent completely at high electric fields.

There are two possible explanations for the suppression of the Mu_{BC}^0 signal by the external electric field. The first possibility is ionization of an initially bound muonium centre by the applied field. Alternatively, the track electrons and the muon may be

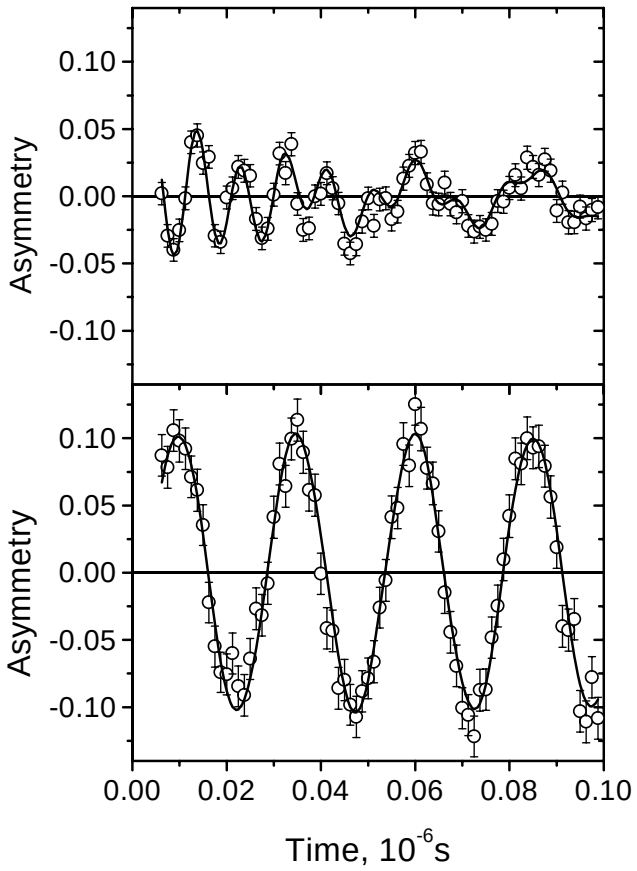

Fig. 65. Experimental μSR spectra in intrinsic GaAs at $T = 10$ K in transverse magnetic field $B = 3000$ G. Top: zero electric field. The theoretical curve is the sum of several muonium frequencies plus a small diamagnetic signal. Bottom: high external electric field (20 kV/cm). Only the diamagnetic signal is present.

initially separated, in which case the external electric field prevents electron transport to the muon.

The characteristic electric field ($E_{\rm char}$) required to change the diamagnetic/muonium fraction significantly is measured to be about 5 kV/cm in semi-insulating GaAs [Eshchenko *et al., op. cit.*]. To ionize ground-state Mu^0_{BC} muonium, much higher electric fields (atomic scale) would be required. On the other hand, in GaAs a positive ion and a light electron in the Γ-valley ($m^* \sim 0.07 m_e$) can form a weakly bound ($U = -7 \times 10^{-3}$ eV) macroscopic-sized ($a_0 = 8.3 \times 10^{-7}$ cm) shallow donor state [Animalu, Intermediate Quantum Theory of Crystalline Solids (Prentice-Hall, Englewood Cliffs, N.J., 1977)]. The electric field E_i required to ionize this state can be estimated by equating the bias across the orbit, $2eE_ia_0$, to the binding energy [Knox, Theory of Excitons (Academic Press, New York, 1963)]. This rough estimate gives $E_i \sim 5$ kV/cm in good agreement with the $E_{\rm char}$ observed experimentally. Thus the model of electric field induced ionization suggests ionization from the shallow state, which in this picture is a metastable precursor for the observed Mu states.

In the alternative model one should consider initially separated free electrons moving (under the influence of the combined Coulomb and external electric fields) to the muon and/or to parent positive ions. At low temperature, where the electron mobility is very high, this motion is ballistic rather than the "classical" viscous flow behaviour. Assuming a Coulomb potential between the electron and the muon, from the characteristic field one can estimate the typical length scale of the interaction: $R_{\rm char} \sim \sqrt{e/(\epsilon E_{\rm char})} \sim 10^{-6}$ cm, where $\epsilon = 11.6$ is the dielectric constant of GaAs. On the other hand, the mean free path of a band electron in GaAs at 50 K is estimated to be $\ell = (b/e)\sqrt{3kTm^*} \sim 6 \times 10^{-6}$ cm (where $b \sim$ 1-2×10^4 cm^2/V$\cdot$ s is the electron mobility), i.e. greater than $R_{\rm char}$. From this estimate it is clear that even if an electron starts far from the muon, in the process of recombination it will eventually form (or at least pass through) the macroscopic size shallow quantum state mentioned above. An external electric field will bias the potential shape. In a weak external electric field, the electron falls to the muon through the shallow state. If the external electric field is higher than E_i the precursor shallow bound state never forms, the electron escapes capture and is lost. Thus, in this model an electric field of about E_i will prevent muonium formation with an initially separated track electron.

We report the direct evidence that the formation of the Mu^0_{BC} muonium centre in GaAs proceeds via transport of initially separated (to distances of more than 3×10^{-6} cm) excess electrons to the muon. To prove this we carried out experiments in GaAs samples with Cr impurities. The idea of the experiment was to place an impurity between the electron and the muon and thus influence electron transport to the muon.

Time-differential μSR experiments were performed on the M20 surface muon channel at TRIUMF. We tested two samples: a clean "intrinsic" GaAs sample with $n_{\rm Cr} < 5 \times 10^{15}$ cm^{-3} and a sample with $n_{\rm Cr} = 3 \times 10^{16}$ cm^{-3} and a defect density of $n_d < 5 \times 10^4$ cm^{-3}. Experimental data were obtained using a newly developed technique of μSR measurements in frequently switched external electric fields [Eshchenko *et al., op. cit.*].

From the experiments in high transverse magnetic field [[Eshchenko *et al., op. cit.*], it is known that the decrease with electric field of the Mu^0_{BC} signal is accompanied by a corresponding increase of the diamagnetic amplitude. This fact is illustrated at the top of Fig. 66. New experiments were performed in a weak transverse magnetic field of 100 G. At that field the Mu^0_{BC} signal relaxes too fast to be observed and the

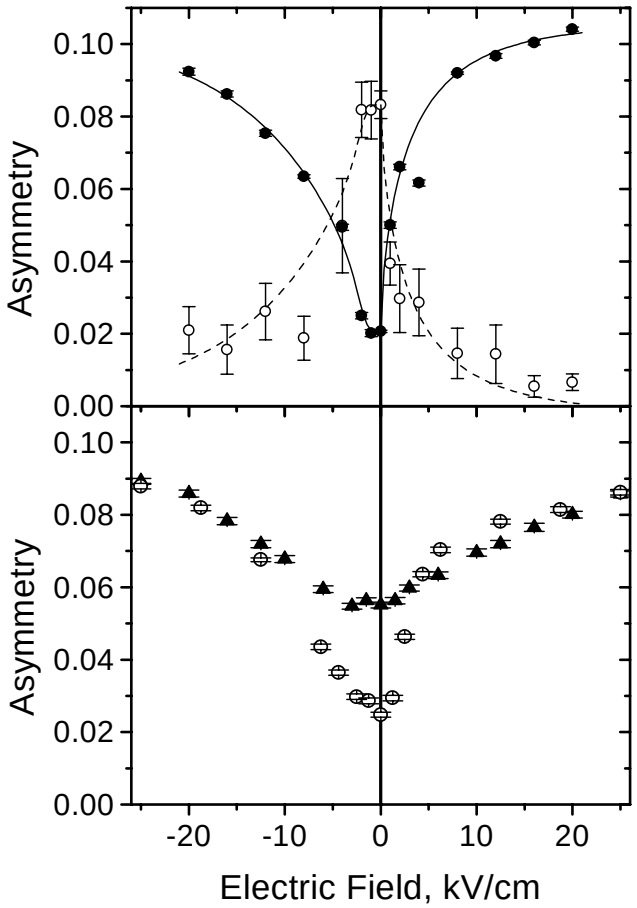

Fig. 66. Top: electric field dependence of the diamagnetic asymmetry (filled circles) and the sum of Mu^0_{BC} asymmetries (open circles) in GaAs at $T = 10$ K. Positive electric field is in the direction of the initial muon beam momentum. The half-period of the alternating electric field is 0.005 s. The lines are to guide the eye. Bottom: electric field dependence of the diamagnetic asymmetry at $T = 50$ K in GaAs with $n_{\rm Cr} < 5\times10^{15}$ cm^{-3} (circles) and $n_{\rm Cr} = 3\times10^{16}$ cm^{-3} (triangles). The half-period of the alternating field is 5 s. In both experiments the temperature was lower than the ionization temperature of shallow states ($U \sim 80$ K).

Mu^0_T frequencies are too high for the finite timing resolution of the spectrometer; thus the only observable signal is the diamagnetic one. Bearing in mind the results in high magnetic field (see top of Fig. 66), experiments in weak magnetic field give complete information about Mu^0_{BC} formation.

The electric field dependence of the diamagnetic amplitudes in GaAs samples with *Cr* impurities at $T = 50$ K is shown at the bottom of Fig. 66. One can notice a remarkable difference between these dependences at low fields $|E| < 10$ kV/cm, while at high fields the data practically coincide. A possible explanation of the different behaviour of the electric field dependence in the dirty sample in low fields could be the following. The characteristic distance between Cr centres in the dirty sample is $R_{\rm Cr} = n_{\rm Cr}^{-1/3} \sim 3\times10^{-6}$ cm. This value is higher than the radius $a_0 = 8.3\times10^{-7}$ cm of the shallow donor state which we suggest is a precursor state for the ground state of Mu^0_{BC} in GaAs. Then in the dirty sample, Cr impurities can scatter or even capture track electrons which where initially located at a distance greater than $R_{\rm Cr}$ from the stopped muon, and the probability of muonium formation will be less than that in the "pure" crystal.

On the other hand, electric fields stronger than $E_i \sim 5$ kV/cm will prevent the muon and electron from coming together regardless of the presence of impurities and the probability of muonium formation in any sample of GaAs will be almost the same.

The electric field dependence in the "pure" sample is almost the same as that measured in the semi-insulating sample (see Fig. 66). This fact implies that up to some level of impurity concentration (about 10^{15} cm^{-3}) the process of muonium formation is independent of the small amount of impurities.

In conclusion, we have used the new μSR technique of measurements in alternating electric fields to study the influence of Cr impurities on short range transport of excess electrons to μ^+ centres in GaAs. Our results suggest that Mu^0_{BC} formation proceeds via electron transport to the stopped muon. Just after muon implantation into the sample, the muon and its track electrons are separated by distances greater than $R_{\rm Char} \sim 3\times10^{-6}$ cm. Under the influence of Coulomb attraction, track electrons approach the muon and/or their parent positive ions. For Cr concentrations greater than about $n_{\rm Cr} \sim 10^{16}$ cm^{-3}, an electron can be captured/scattered by Cr impurities on its way to the muon. Those electrons which avoid scattering by Cr impurities may form a short lived shallow state with radius $a_0 \sim 10^{-6}$ cm – the precursor of the ground state of Mu^0_{BC}. External electric fields higher than $E_i \sim 5$ kV/cm prevent formation of this shallow state, thus diminishing the probability of Mu^0_{BC} formation.

Experiment 776
Rare-earth materials with disordered spin structures
(D.R. Noakes, Virginia State)

This experiment was a muon spin relaxation (μSR) study of RE-Mg-Zn (RE=rare earth) quasicrystals and PrP_x induced moment "spin glasses", as described in several previous Annual Reports. A paper on Monte Carlo simulations of the singlet-ground "crystalline electric field" (CEF) level fluctuation model for the observed μSR in PrP_x, described in previous Annual Reports, has been submitted to the Journal of Physics: Condensed Matter.

In the paramagnetic state (above the freezing temperature) of the Tb-Mg-Zn quasicrystal, monotonic

but non-exponential ZF-μSR was observed. This was of form and temperature dependence observed in a number of disordered dense-moment magnetic materials. In the past, this form had been described in terms of phenomenological "power-exponential" relaxation

$$G_z(t) = \exp\left[-(rt)^p\right]$$

where r is a relaxation rate and the power p is near 1.0 (exponential relaxation) far above the magnetic freezing temperature, but falls as temperature is lowered, to values of 0.5 or less as the freezing temperature is approached [see, for example, Campbell *et al.*, Phys. Rev. Lett. **72**, 1291 (1994)]. ZF-μSR in the paramagnetic Gd-Mg-Zn quasicrystal was exponential, however, except perhaps just above the freezing [both quasicrystal measurements were reported in Noakes *et al.*, Phys. Lett. **A238**, 197 (1998)]. There is no direct physical interpretation of power-exponential relaxation unless p is exactly 1.0 or 0.5 (the latter occurs for dilute spin glasses in the fast-fluctuation limit). It had been suggested that varying-power exponential relaxation is caused by a wide variety of moment fluctuation rates in the material [Heffner *et al.*, Phys. Rev. Lett. **77**, 1869 (1996)], but without detailed justification, until now. In a manuscript accepted for publication in Phys. Rev. B, we begin with a simple, broad, "double-square" distribution of exponential relaxation rates, representing a large number of muon sites in a material, each muon site experiencing a different local-field fluctuation rate. We integrate over the distribution to find a new analytic ZF muon spin relaxation function

$$G_{dsq}(t) = \frac{(w+1)e^{-\lambda_0 t/(w+1)} - we^{-\lambda_0 t} - e^{-(w+1)\lambda_0 t}}{2w\lambda_0 t},$$

where λ_0 is the average relaxation rate in the distribution and w is a dimensionless width (the maximum relaxation rate in the distribution divided by the average). This relaxation function fits the ZF-μSR data from the paramagnetic Tb-Mg-Zn quasicrystal, and corresponding data from paramagnetic amorphous DyAg [TRIUMF Expt. 347, originally reported in Hyp. Int. **31**, 303 (1986)], at least as well as the power-exponential relaxation function does, and the deduced parameters can be interpreted physically. We show that for the Tb-Mg-Zn quasicrystal and for *am*-DyAg, the wide distribution of moment fluctuation rates can be attributed to widely, randomly-varying rare earth CEF coupling strengths (not just randomly-varying CEF easy-axis directions), caused by the disorder in the materials. That then automatically explains why only exponential ZF relaxation was observed in the Gd-Mg-Zn quasicrystal: gadolinium is an s-state, spherical ion, unaffected by the CEF.

Experiment 782
Non-fermi-liquid behaviour and other novel phenomena in heavy-fermion alloys
(D.E. MacLaughlin, California, Riverside)

Non-Fermi liquids and heavy-fermion superconductors

The observed breakdown of Landau's Fermi liquid paradigm in a number of metallic systems, among them certain f-electron heavy-fermion materials, has led to an explosion of effort to understand this non-Fermi liquid (NFL) behaviour. From the outset a number of mechanisms have been proposed to explain NFL phenomena; most work has concentrated on effects of a quantum critical point (QCP) separating magnetically ordered and paramagnetic phases at zero temperature. Early theories ignored the fact that most heavy-fermion alloys exhibiting such phenomena ($Y_{1-x}U_xPd_3$, $UCu_{5-x}Pd_x$, ...) were disordered by chemical substitution.

After our NMR linewidth measurements in UCu_4Pd and $UCu_{3.5}Pd_{1.5}$ demonstrated that the magnetic susceptibility in these materials was strongly inhomogeneous, two broad classes of theories began to address the role of disorder in NFL behaviour. In the "Kondo-disorder" approach, interactions between f moments are ignored and structural disorder gives rise to a broad distribution of Kondo temperatures T_K; NFL behaviour arises from low-T_K spins which are not in the Fermi-liquid state. In the "Griffiths-phase" picture, spin-spin interactions freeze low-T_K f moments into clusters with a wide distribution of sizes; the larger clusters dominate the susceptibility and lead to divergent behaviour as the temperature is lowered. Both Kondo-disorder and Griffiths-phase scenarios seem to be compatible with observed μSR and NMR linewidths.

Recent μSR spin-lattice relaxation experiments in $UCu_{5-x}Pd_x$ indicated, however, that the U-ion spin dynamics are better described by a cooperative picture in which critical slowing down occurs throughout the sample, rather than at (rare) low-T_K spins or large clusters. The μSR relaxation rates are nevertheless widely distributed, and the dynamic behaviour closely resembles that of spin glasses. Thus an important question is whether the appropriate model is one in which disorder in the interactions dominates the dynamics, as in a spin glass above the glass temperature, or if, instead, the critical slowing down is still controlled by a QCP. Theoretical treatments exist which combine elements of both these viewpoints and describe a "quantum spin glass" with a suppressed or possibly zero glass temperature.

We have begun preliminary μSR measurements

on a novel praseodymium-based heavy-fermion superconductor, the "filled skudderudite" compound $PrOs_4Sb_{12}$. This material has a relatively high transition temperature, $T_c = 1.85$ K, and a large effective mass, $m^* \approx 50m_e$. The intriguing aspect of this particular compound is that the Pr^{3+} ion may possess a nonmagnetic doublet Γ_3 crystal-field ground state, in which case the usual spin-based Kondo model is not applicable and the system is expected to be a "quadrupolar Kondo" non-Fermi liquid.

The goals of our μSR studies of novel heavy-fermion materials are (a) to clarify the nature of the mechanism or mechanisms responsible for NFL behaviour under a variety of circumstances, and (b) to determine whether novel nonmagnetic heavy-fermion states are involved in praseodymium-based systems, particularly heavy-fermion superconductors.

Progress to date

UCu_4Pd

In previous work we have studied local f-electron spin dynamics in the non-Fermi-liquid heavy-fermion alloys $UCu_{5-x}Pd_x$, $x = 1.0$ and 1.5, using muon spin-lattice relaxation. The sample-averaged asymmetry function $\overline{G}(t)$ indicates strongly inhomogeneous spin fluctuations, and exhibits the scaling $\overline{G}(t,H) = \overline{G}(t/H^\gamma)$ expected from glassy dynamics. At 0.05 K $\gamma(x{=}1.0) = 0.35{\pm}0.1$, but $\gamma(x{=}1.5) = 0.7{\pm}0.1$. There is no sign of static magnetism $\gtrsim 10^{-3}$ μ_B/U ion in either material above 0.05 K. Our results strongly suggest that both alloys are quantum spin glasses. In UCu_4Pd the scaling exponent γ is small and temperature independent. In $UCu_{3.5}Pd_{1.5}$, γ varies with temperature, increasing with decreasing temperature similar to spin-glass AgMn. This suggests that the spin-glass state found for $x \gtrsim 2$ in $UCu_{5-x}Pd_x$ modifies the low-frequency spin dynamics in $UCu_{3.5}Pd_{1.5}$. In both alloys, γ extrapolates to high temperatures in agreement with neutron scattering experiments.

Our collaborators at the University of Augsburg have reported specific heat $C(T)$ and resistivity $\rho(T)$ data from annealed and unannealed samples of UCu_4Pd. They found that a thorough annealing treatment modifies both $C(T)$ and $\rho(T)$, the latter drastically; the residual resistivity is reduced considerably and, more surprisingly, the T-linear behaviour of $\rho(T)$ at low temperatures is lost. The authors suggest that NFL behaviour in the annealed material is not driven by disorder and, by extension, that disorder is not involved in the unannealed materials either.

We therefore carried out relaxation measurements at low temperatures in annealed and unannealed samples of UCu_4Pd supplied by E. W. Scheidt, University of Augsburg. The data showed disorder in the spin dynamics of both samples; with similar values of the exponent γ. The measured relaxation rates were, however, about a factor of seven slower in the unannealed sample. No trace of magnetic ordering was found in either sample. This study has not been published to date, since our German collaborators have indicated that their annealing treatment was not successful in arriving at a sample with properties as previously reported. We are awaiting development of appropriate annealing techniques for the considerably larger specimens required for μSR experiments.

$Ce(Ru_{0.5}Rh_{0.5})_2Si_2$

This NFL alloy had previously been identified as possessing a disorder-driven NFL mechanism from thermodynamic measurements and a ^{29}Si NMR study. But these NMR experiments were carried out in powder samples. The possibility has been raised that disorder introduced in the powdering process, or possibly in the original fabrication of the sample, was responsible for the NMR results, and that the mechanism for NFL behaviour in this system is not driven by disorder. We therefore obtained an extremely well-characterized single-crystal sample of $Ce(Ru_{0.5}Rh_{0.5})_2Si_2$ from the group of Y. Myako at Osaka University. NMR on single crystals is difficult due to the small skin depth for radio frequency signals, but no such problem exists for μSR. Furthermore, the NMR experiment used field-aligned, epoxy-potted samples, which would not be suitable for μSR because a large fraction of the muons would stop in the epoxy. The single crystal $Ce(Ru_{0.5}Rh_{0.5})_2Si_2$ sample was therefore ideal for a μSR study.

Analysis of the bulk susceptibility of such a crystal in the framework of disorder-driven Griffiths-phase and Kondo-disorder models for NFL behaviour yields relatively narrow distributions of characteristic spin fluctuation energies, in agreement with μSR linewidths that give the inhomogeneous spread in susceptibility. μSR and NMR data both indicate that disorder explains the "nearly NFL" behaviour observed above $\sim$2 K, but does not dominate the NFL physics found at low temperatures and low magnetic fields. A paper on these results has been published.

$PrOs_4Sb_{12}$

Heavy-fermion behaviour has been reported in a small number of praseodymium-based alloys and compounds. Pr^{3+} is a non-Kramers ion; if the crystal-field ground state is nonmagnetic and degenerate, a charge-scattering analogue of Kondo spin scattering can take place and give rise to the so-called "quadrupolar Kondo effect." This can occur for a doublet Γ_3 CEF ground state, although the degeneracy could be lifted by a cooperative Jahn-Teller effect. It seems possible, though,

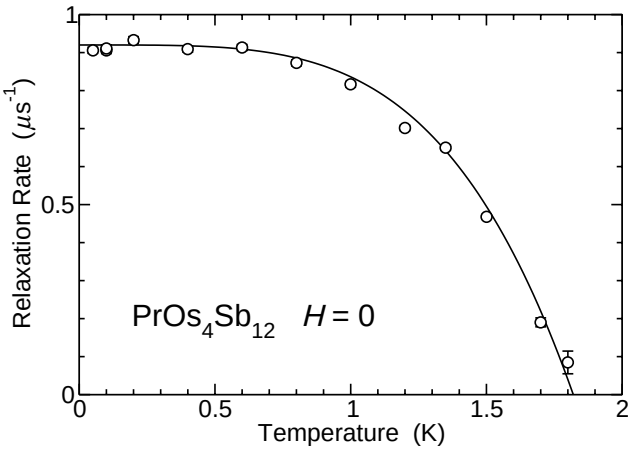

Fig. 67. Temperature dependence of vortex-state μ^+ relaxation rate $\sigma_s(T)$ in the superconducting state of $PrOs_4Sb_{12}$. Curve: fit to $\sigma_s(T) = \sigma_s(0)[1-(T/T_c)^4]$; $\sigma_s(0) = 0.92$ μs^{-1}, $T_c = 1.83$ K.

that the observed heavy-fermion behaviour and superconductivity in $PrOs_4Sb_{12}$ is associated with an unconventional "nonmagnetic" heavy-fermion state.

Initial results for the superconducting vortex-state relaxation rate $\sigma_s(T)$ are given in Fig. 67. The zero-temperature value $\sigma_s(0) \approx 0.9$ μs^{-1} yields an estimated London penetration depth $\lambda(0) \approx 3500$ Å, which is quite short for a heavy-fermion superconductor. The data are consistent with the "two-fluid" temperature dependence $\sigma_s(T) = \sigma_s(0)[1-(T/T_c)^4]$. The lack of temperature dependence of $\sigma_s(T)$ at low temperatures suggests that we are dealing with an s-wave (or possibly p-wave) superconductor, but the data are very preliminary.

Experiment 783
Knight shifts in unconventional superconductors: (U,Th)Be_{13}
(G.D. Morris, LANL)

Introduction

Experiment 783 is investigating unconventional superconductivity in the $U_{1-\delta}Th_\delta Be_{13}$ heavy-fermion materials. Muons in these cubic materials occupy a single crystallographic site midway between U atoms. However, the application of an external magnetic field generates *magnetically* inequivalent sites due to the presence of field-induced $5f$ moments. With a magnetic field along the c axis, the two sites in the $a-b$ plane are equivalent and situated such that the dipolar fields from the nearest $5f$ U moments subtract from the applied field. These are termed the perpendicular sites with negative Knight shift $K_\perp$. For the site between U moments arranged along the field, the shift $K_\parallel$ is positive. Overall, the resulting characteristic spectrum has one line shifted down from the silver reference line, and a line with twice as much intensity shifted up in

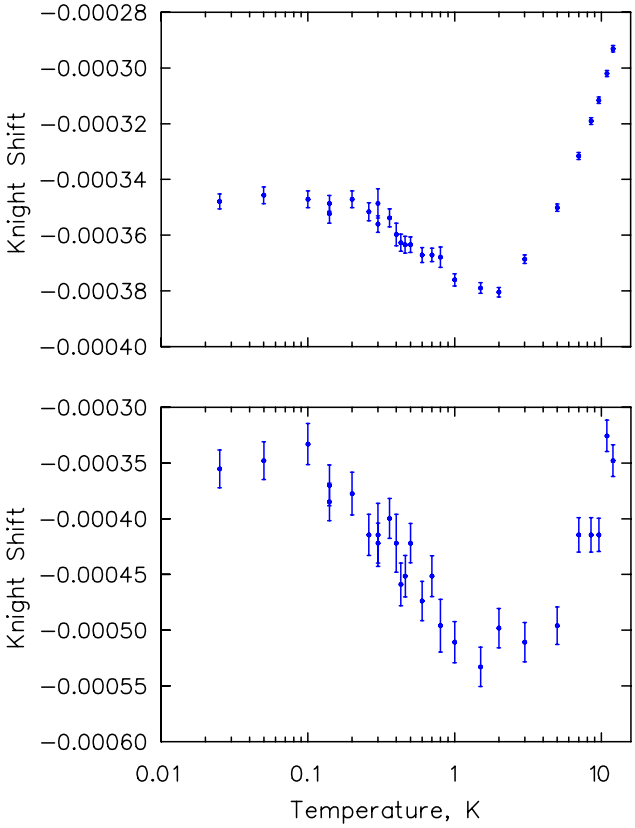

Fig. 68. Knight shifts at two magnetically inequivalent muon sites in $U_{0.965}Th_{0.035}Be_{13}$, with the sample oriented with (011) at 45° to the 1 T magnetic field.

frequency. Given the crystal structure, the magnitude and sign of the shifts and signal amplitudes unambiguously determine the muon sites.

In addition to the dipolar term, there is an RKKY interaction coupling the induced moment on the U atoms to the muon spin. Since the frequency shifts for the different sites are related, it is possible to unravel these various contributions to the Knight shift, yielding the pair spin susceptibility $\chi_s(T)$ and hyperfine contributions to the Knight shift.

Substitution of a small amount of Th for U in UBe_{13} is known to produce a second peak in the specific heat at $T_{c2} < T_{c1}$, which is consistent with the onset of a second superconducting order parameter. Previous experiments performed under Expt. 783 measured the muon Knight shifts in $U_{0.965}Th_{0.035}Be_{13}$ with the magnetic field applied along crystal axes. The principal finding of those experiments was the observation that the spin susceptibility probed by the muon drops with T between T_{c1} and T_{c2}, below which it remains constant [Sonier *et al.*, Phys. Rev. Lett. **85**, 2821 (2000)]. This is in contrast to the situation in pure UBe_{13} where the spin susceptibility continues to drop with temperature toward T = 0. It was also found

that in the normal state the hyperfine coupling between muon spin and $5f$ electrons is anisotropic in both Th-doped and pure UBe_{13}.

Status of Expt. 783

In 2001 we began experiments to study the anisotropy of the Knight shift in $U_{0.965}Th_{0.035}Be_{13}$. Low temperature data (0.025 K < T < 12 K) were collected with the external magnetic field oriented along the (110) direction in the cubic lattice. We plan to take additional data over a range of higher temperatures to complete the data set necessary for the analysis of the Knight shift in the superconducting state.

Experiment 784
Spin dynamics in the two dimensional spin system $SrCu_2(BO_3)_2$
(A. Fukaya, Y.J. Uemura, Columbia)

The spin arrangement of $SrCu_2(BO_3)_2$ is topologically identical to the Shastry-Sutherland model, in which the ground state is an exact dimer state. The magnetic susceptibility decreases at low temperatures indicative of the spin gap (Δ=34 K) associated with a singlet pair formation of dimers.

We have performed muon spin relaxation measurements in the pure and diluted $SrCu_2(BO_3)_2$. Figure 69 shows the temperature dependence of the zero-field μSR time spectra. As the temperature decreases, the relaxation rate increases below T=10 K, and shows a saturation below T=3 K. The line shape at low temperatures is nearly Gaussian, yet it cannot be easily decoupled by an application of longitudinal field, as shown in Fig. 70. These results indicate the existence of magnetically active spins which show slowing down of fluctuations with decreasing temperatures, yet remaining dynamic even at

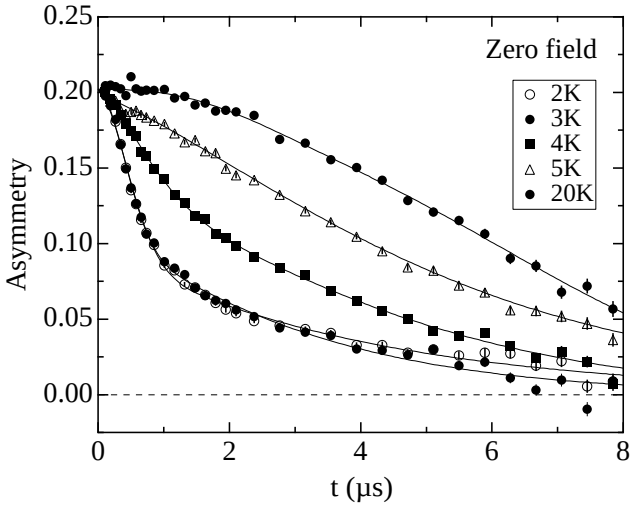

Fig. 69. Temperature dependence of the time spectra in zero-field.

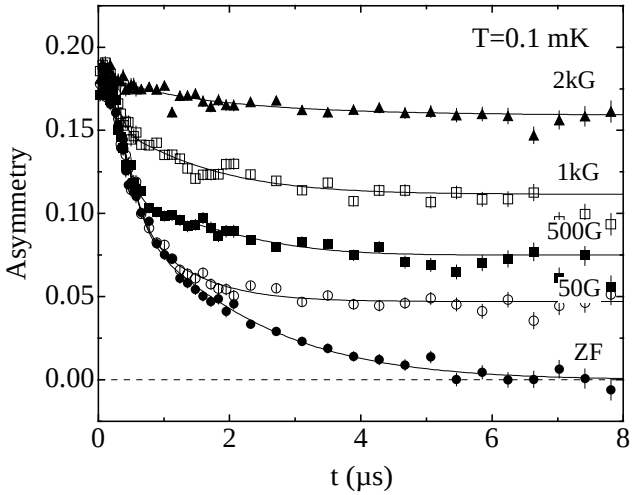

Fig. 70. Longitudinal field dependence of the time spectra at T=0.1 K.

0.1 K. The present results are similar to the observation of muon spin relaxation in widely-believed spin gap systems, such as NaV_2O_5 and CaV_4O_9. The "undecouplable-Gaussian" line shape is common to μSR results in the kagomé lattice and other geometrically frustrated spin systems. In a diluted system where 1% of Cu is substituted by non-magnetic Zn, we observed μSR results essentially identical to those in pure $SrCu_2(BO_3)_2$. This indicates that the observed spin relaxation is not due to impurity spins.

Experiment 791
Electronic structure and dynamics of charged muonium centres in semiconductors
(K.H. Chow, Alberta; B. Hitti, TRIUMF; R.F. Kiefl, UBC)

Results of experiments on muonium are generally considered to be the main source of information on isolated hydrogen in semiconductors. Hydrogen is an important impurity which can dramatically affect the electrical and optical properties of these technologically relevant materials. Recently, we published our observation of the reaction between Mu^+ and the substitutional Zn dopant in heavily doped GaAs:Zn [Chow *et al.*, Phys. Rev. Lett. **87**, 216403 (2001)]. This was the first atomic scale study of the formation of a hydrogen or hydrogen-like complex, as it happens, with an intentional impurity in a semiconductor. An important extension of these studies is the sub-nanoscopic characterization of the electronic structure of the isolated precursor state that is seen at low temperature. Such information is interesting for several reasons. First, it enables comparisons with the many theoretical calculations on the subject, which generally place the positively charged muon or proton at or near a distorted bond-centre position. Thus far, there has been no experimental evidence on the stucture of H^+ or Mu^+ in a

semiconductor. Second, structural information on the isolated state will help us understand how the muon or hydrogen makes a transition from its percursor configuration to being part of a complex.

Information on the structure of a diamagnetic centre such as Mu^+ is obtained by studying the dipole and muon-induced quadrupole interactions with the host Ga and As nuclei, all of which have spin 3/2. The most powerful technique for this purpose is avoided level crossing (ALC), often called μLCR. In this method, a dip (also called a resonance) in the integrated muon polarization appears at values of **B** where resonant cross-relaxation between the muon and neighbouring nuclear spins occurs due to avoided level-crossings in the combined energy levels. The positions of the resonances associated with a particular nucleus are determined primarily by Q and to a smaller extent by θ, often giving a distinct fingerprint that identifies the neighbouring nucleus and its symmetry. Recall that Q is the strength of the quadrupole interaction and θ is the angle between the applied magnetic field and the muon-nucleus direction.

We have recently completed our investigations of the structure and location of the precursor isolated Mu^+ state mentioned above. Figure 71a summarizes the relevant results of our μLCR experiments in a heavily doped p-type GaAs:Zn sample at 50 K with **B** $||\langle 100\rangle$. At this temperature, the isolated Mu^+ centre is static. Only the regions where resonances are observable are shown. (These experiments are performed with field modulation, hence the derivative-like signals.) The two lower field resonances, located at ≈1.9 and ≈3.0 kG, can be unambiguously assigned to a nearest neighbour Ga atom. This is because the ratio of their positions is identical to the ratio of the ^{69}Ga and ^{71}Ga quadrupole moments (0.168×10^{-24} e.cm^2 and 0.106×10^{-24} e.cm^2). This is further confirmed by Fig. 71b, which shows theoretically the expected resonances. A single value of the electrical field gradient was used to produce this figure. (Note that for each Ga isotope, the signal-to-noise is too low to experimentally resolve the weaker of the pair.) On the other hand, the higher field resonances (≈6.4 and ≈7.35 kG are certainly due to an As atom (^{75}As, 100% abundant, I=3/2), the only other atom in the host species in the lattice that can produce μLCR resonances. The unambiguous identification of Ga and As as nearest neighbors of Mu^+ is certainly a very important breakthrough. However, a crucial piece of information is still lacking, namely how these atoms are oriented with respect to the muon. This information is obtained by performing μLCR experiments (not shown) at other major crystalline orientations, namely with **B**$||\langle 110\rangle$ and **B**$||\langle 111\rangle$. The positions and strengths of the lines

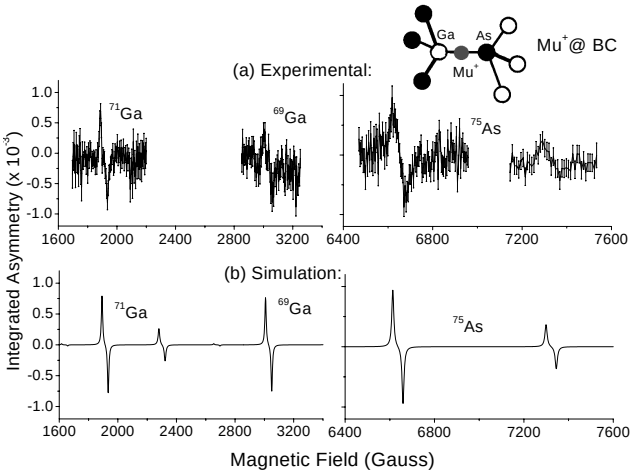

Fig. 71. (a) μLCR at 50 K in heavily doped p-type GaAs:Zn with **B**$||\langle 100\rangle$. (b) Theoretical simulation as described in the text.

in Fig. 71a change in a manner that unambiguously confirms that the muon, the Ga, and the As atoms all lie on the same $\langle 111\rangle$ axis (i.e. $\theta = 54.7°$).

Thus, our results provide strong evidence that Mu^+ is located near the centre of a Ga-As bond, as indicated in Fig. 71. Finally, we note that contained in our μLCR data is another piece of important information, namely the distances between Mu^+ and the neighbouring Ga and As nuclei. We are currently in the process of extracting this information.

Experiment 804
Muonium in III-V nitrides
(R.L. Lichti, Texas Tech)

The goal of TRIUMF Expt. 804 is to investigate the muonium analogue of hydrogen defect states in GaN and other group-III nitrides. During the past year we obtained the full temperature dependence of the QLCR resonances for several samples of AlN. These data represent diamagnetic Mu^+ centres and show features related to their sites and dynamics. The likely stable Mu^+ sites are nitrogen anti-bonding locations oriented into the channels formed by the 2H Wurtzite stacking order, commonly noted as $AB_\perp$[N]. The other likely site is a second anti-bonding location with Mu^+ inside the most tightly confined cage region of the structure. The strong QLCR line in Fig. 72 is assigned to this metastable $AB_\parallel$[N] cage site. This signal is strongest in AlN samples with smallest grain sizes or otherwise highly defective.

The QLCR spectra from fine-grained polycrystalline AlN look very similar to that for the CVD film in Fig. 72, but with broader lines due to small anisotropies and splittings. Preliminary results from zero-field relaxation signatures assigned to the static $AB_\parallel$[N] cage sites and the more mobile $AB_\perp$[N] sites

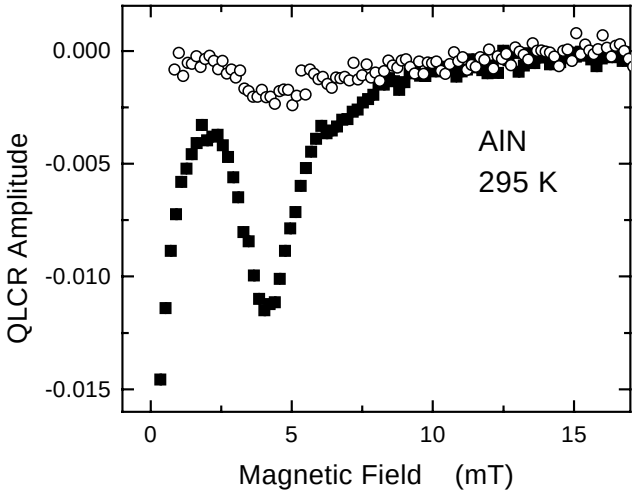

Fig. 72. Comparison of QLCR spectra from two AlN samples: a *c*-axis oriented CVD film (filled symbols) and a single crystal sample (open symbols). Differences imply that the metastable $AB_{\|}$ state is less likely in better material.

had already suggested that the trapped cage state is preferentially formed in more defective material. The single crystal QLCR spectra verify this conclusion.

We will need relaxation data and QLCR spectra at other temperatures for good single crystal AlN to draw any firm conclusions regarding Mu^+ dynamics in the best material. The following discussion provides a brief update on our present understanding of Mu^+ dynamics in AlN from data on polycrystalline bulk samples and oriented films produced by a variety of techniques. The cage sites are populated in all of these samples, but the fractions vary widely and appear correlated with visual sample quality.

The results shown in Fig. 73 are from bulk polycrystalline AlN. The oriented films give very similar dynamics for the cage site, but show large variations in features assigned to Mu^+ channel states. At the highest temperatures the main 4.1 mT resonance broadens and decreases in amplitude characteristic of either motion or disappearance of the metastable cage site. We associate this broadening with motion of Mu^+ out of the $AB_{\|}$ site into the mobile channel $AB_{\perp}$ states. The barrier for this transition appears to be approximately 1.0 eV from both the QLCR results (Fig. 73) and from zero-field depolarization data. A Kubo-Toyabe zero-field component was earlier correlated with the strong QLCR line, and gave a Mu^+ site change barrier ranging from about 0.9 to 1.1 eV depending on the precise value chosen for the static KT width [Lichti *et al.*, Physica **B**, in press].

An interesting outcome from these fits is that the linewidths associated with both the zero-field non-resonant component and the 6 mT resonant feature decrease as the amplitudes decrease at high temperature. At the moment this narrowing is not fully

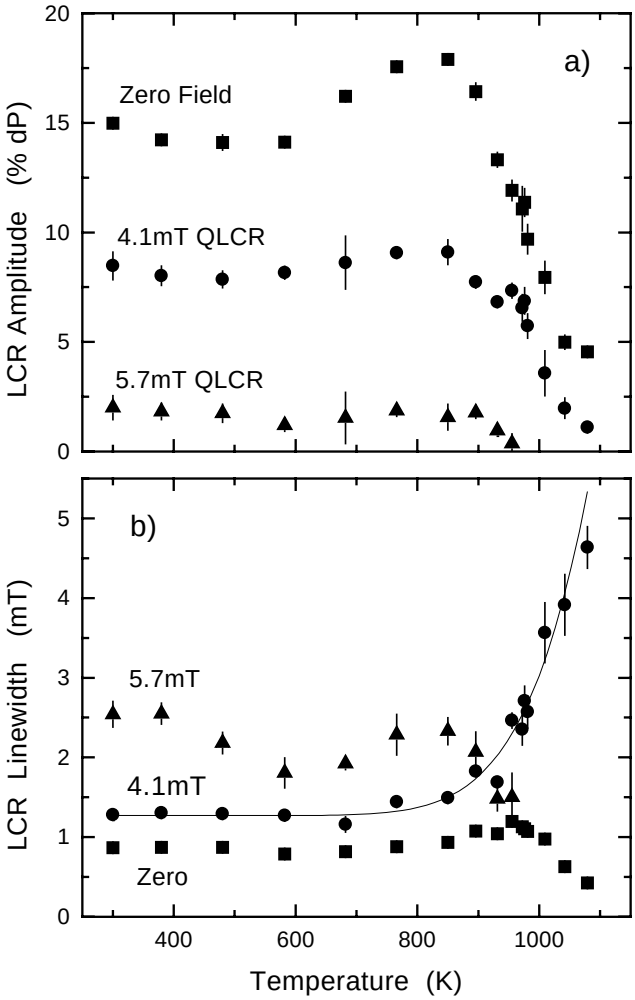

Fig. 73. Parameters from fits to QLCR spectra for polycrystalline AlN, including the non-resonant depolarization near zero field. The high-T increase in width of the 4.1 mT line yields a 0.99±0.12 eV barrier for the Mu^+ site change from $AB_{\|}$[N] to $AB_{\perp}$[N].

understood, but may be related to a change in diffusion and associated averaging of electric field gradients related to the mobile Mu^+ channel states. The change in width near 600 K for the weaker higher field line is correlated with a decrease in relaxation rate for the depolarization component tentatively assigned to the mobile Mu^+ centres, suggesting that this line and the weakly relaxing zero-field component are in fact from the same states.

Late in the year with time shared between Expt. 804 and Expt. 865, several *n*-type GaN samples were examined in Belle at 3 T to search for a Mu^0 precursor to one of the observed diamagnetic states. Such a precursor was implied below 50 K by earlier relaxation measurements. A small crystal film, *n*-type at 10^{16}cm^{-3} obtained from NEC [Expt. 865 sample], showed beats implying a small hyperfine splitting along with a fast exponentially relaxing diamagnetic signal.

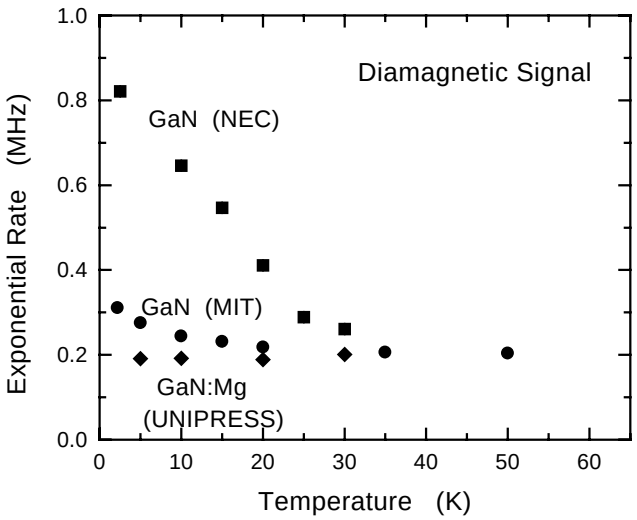

Fig. 74. The temperature dependent exponential relaxation rates for the NEC GaN sample (squares), HVPE thick film MIT GaN sample (circles), and Mg doped GaN single crystal from UNIPRESS (diamonds). The latter relaxation is actually Gaussian, even at the lowest temperatures.

The splitting is characteristic of a shallow donor Mu^0 state as observed in several II-VI compounds and predicted for InN. Two of the Expt. 804 samples were similarly examined. A c-axis oriented film, grown by HVPE methods at MIT and having the same n-type concentration, showed similar characteristics although a slower diamagnetic relaxation rate obscured visibility of the beats. However, a small single crystal, obtained from UNIPRESS, doped with Mg to compensate the natural n-type character of GaN showed no sign of either the Mu^0 state or the exponentially decaying diamagnetic signal. Figure 74 shows the low-T diamagnetic relaxation rates for these three samples.

One possible scenario consistent with this set of measurements is that a shallow donor Mu^0 can be formed from one of the diamagnetic states in sufficiently n-type GaN. This Mu^0 then ionizes at roughly 30 K, based on limited data on the two samples which showed the shallow Mu^0 signature. We suggest that the exponential diamagnetic relaxation might represent e^- capture by a Mu^+, but existing data do not actually identify the original state. We conclude that there is a Mu^0 state at low temperatures in n-type GaN, most likely by delayed formation. Whether the original diamagnetic state and the final state, presumably a Mu^+, following the Mu^0 ionization are the same is yet to be determined.

Experiments 815, 816 and 817: β-NMR

(W.A. MacFarlane, R.F. Kiefl, TRIUMF/UBC)

In the past year we have made significant advances in developing the β-NMR technique at ISAC. A major part of this progress is the successful development of the ^{8}Li optical polarizer, which is described elsewhere in this Annual Report. The main result of this is that we now have available a high spin polarization (50% routinely and up to 70%) in the ^{8}Li beam. In addition we have demonstrated that in a high magnetic field (3 T) we can maintain a well-focused beam while decelerating from 30 keV to at least 1 keV. This was shown by imaging the beam spot with a CCD camera viewing a scintillator target. Advances were also made in understanding the beam transport through the β-NMR optics. The Einzel lenses are now operated in a focus-to-parallel mode minimizing beam "snaking" through the optics and simplifying the field and energy dependence of the beam transport. In addition specific advances in understanding the ^{8}Li β-NMR probe are summarized in the following sections.

Deceleration and range straggling

To demonstrate that we can stop the ^{8}Li beam in a thin structure, we undertook a study of thin noble metal films with the objective of comparing the range straggling to state of the art Monte Carlo calculations embodied in the SRIM2000 program. Noble metals were selected because their simple structure (face-centred cubic) yields simple resonances as we have already found in thick metal foils.

The dramatic contrast in the resonance signals between the metals which have a single narrow resonance near the Larmor frequency and the film substrates

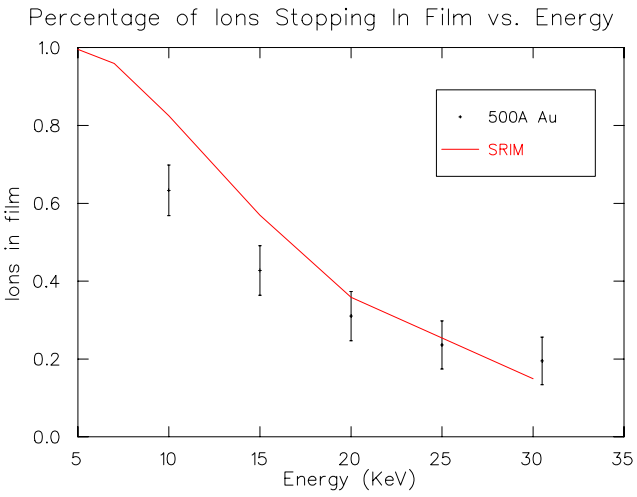

Fig. 75. A comparison of the relative ^{8}Li β-NMR resonance amplitude to the stopping fraction predicted by the SRIM program as a function of the Li beam energy for a 500 Å film of Au.

allowed us to clearly distinguish the signal coming from the thin film. The resonances were observed for several platform voltages, i.e. varying the beam energy from 30 keV down to 1 keV.

Range straggling was performed on a 500 Å Au film on $SrTiO_3$ substrate, using $^8Li^+$. The resulting spectra were appropriately scaled and fit to Gaussians. Amplitudes of these fits were then normalized against spectra at similar energies in an Au foil (which is thick compared to the implantation depth of the $^8Li^+$), and compared to SRIM2000 predictions. It should be noted that this process of normalization against Au foil provides only a lower bound on pecentage of ions stopped in the film. One reason for this is that the resonance is broader in the thin film, possibly a consequence of disorder or a finite-size effect. Future work will involve obtaining spectra in thick Au films (>2000 Å), and normalizing against these spectra instead of the foil spectra.

Thin metallic films

Aside from the demonstration of range straggling presented above, the results in thin metallic films are of interest in their own right. One motivation for this is that thin noble metal films are components of interesting heterostructures such as giant magnetoresistive multilayers. However, we also plan to use them as an integral part of the β-NMR probe in some circumstances. When we are investigating magnetism at the surface of a complex material, our idea is to use the simple ^{8}Li resonance in a thin noble metal overlayer to probe the magnetic field near but outside the sample. One clear reason for this is that the ^{8}Li resonance in a complex material may be complicated, for example, Fig. 76 shows the resonance in a 1000 Å film of the orthorhombic high temperature superconductor YBCO. In such a circumstance it may be easier to extract the interesting information from the simpler overlayer resonance.

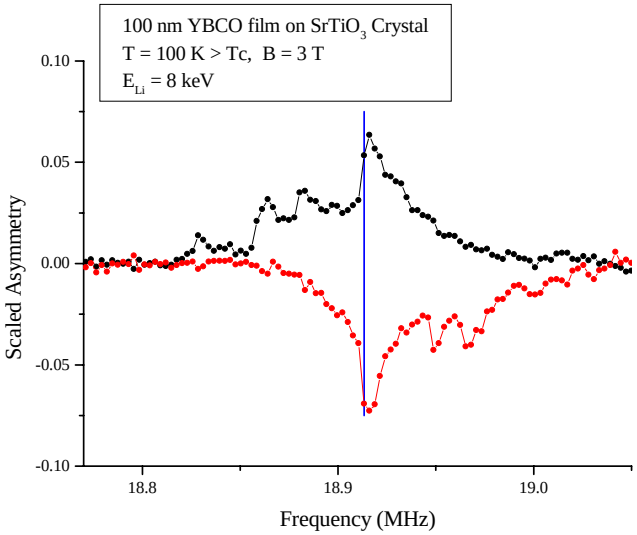

Fig. 76. The ^{8}Li β-NMR resonance in a 1000 Å film of YBCO in the two polarization channels. The line indicates the resonance frequency in MgO.

Initial room temperature measurements of the ^{8}Li β-NMR resonance in the cubic noble metals Ag and Au showed a single narrow line, indicating a single site of cubic symmetry for Li. Surprisingly, as we cooled films of these metals, a second resonance appeared, and grew in amplitude at the expense of amplitude of the high T line. An example of this is shown in Fig. 77. Both lines appear at frequencies higher than the Larmor frequency in an insulator. Specifically in Ag, the two resonances are at +144 ppm and +242 ppm from the resonance frequency in MgO.

These data suggest that there are two distinct sites for Li in the FCC structure of Ag. In this scenario, we ascribe the small positive shifts to a Knight shift, i.e. to a direct coupling of the ^{8}Li nucleus to the Pauli spin susceptibility of the conduction band. This is a common effect in the NMR of metals, yielding significant temperature independent shifts. There are two cubic symmetry interstitial sites in the face-centred cubic lattice, the large octahedral (O) site and the smaller tetrahedral (T) site. Additionally there is the cubic

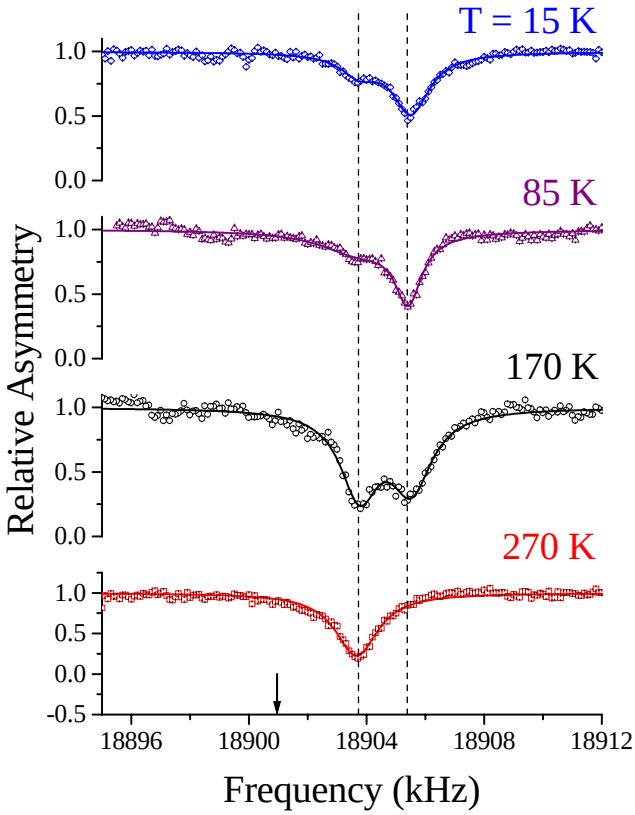

Fig. 77. The temperature dependence of the ^{8}Li β-NMR resonance in a thin film of silver. The two lines correspond to distinct crystallographic sites for Li in Ag. The arrow indicates the resonance position in the insulator MgO.

substitutional (S) site. It is likely that the two observed lines correspond to the O and S sites as the T site is probably too small to accommodate Li. We plan experiments to confirm this scenario in the near future.

In fact this is the first time that the Knight shift has been used to resolve two sites for an implanted β-NMR probe. The reason we are able to accomplish this is the high magnetic field (3 T) used in this measurement. Lower field studies in Cu did not observe such an effect [Ohsumi *et al.*, Hyp. Int. **120-121**, 419 (1999)].

Insulators

Strontium titanate ($SrTiO_3$) is an important substrate material for films of oxide materials such as high temperature superconductors. It is a transparent insulator with the cubic perovskite structure and exhibits a structural phase transition at ∼100 K to a low temperature tetragonal phase. This phase transition has been studied extensively and is considered a prototype of soft-mode structural phase transitions. Interestingly, neutron and synchrotron X-ray diffraction measurements indicate that there is distinct critical behaviour associated with this transition in a region near the surface of the crystal [Hirota *et al.*, Phys. Rev. **B52**, 13195 (1995)].

We have studied ^{8}Li β-NMR in $SrTiO_3$, and find that although it is cubic there is a significant quadrupolar splitting of the lines indicating that the local symmetry of the Li site is non-cubic. Figure 78 shows an example of the resonance in $SrTiO_3$. The electric quadrupole moment of the ^{8}Li nucleus couples the nuclear spin to the electric field gradient (EFG) at the Li site causing the Larmor resonance to be split into a quartet of lines for the spin 2 nucleus. However, the high degree of polarization implies that only the $m = \pm 2$ states are populated appreciably. The applied rf magnetic field can then induce $\Delta m = 1$ transitions, and we will observe only two lines of the quartet. However, instead, we find four lines – two distinct ones in each polarization channel, the inner two having higher intensity.

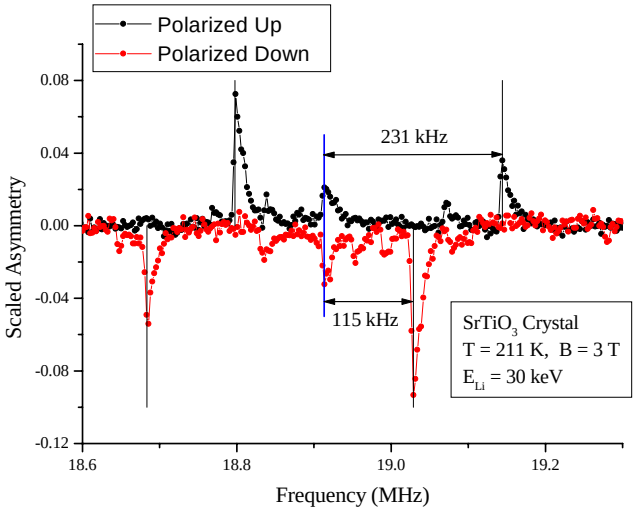

Fig. 78. The ^{8}Li β-NMR resonance in $SrTiO_3$. The central line indicates the Larmor frequency. The resonance is split by the quadrupolar interaction, with a characteristic frequency of $\nu_Q \sim 115$ kHz.

The likely explanation for this effect is that the Li site has a [100] symmetry axis, thus there are in fact three sites with [100], [010] and [001] principal axes in the cubic structure. The field applied along [001] distinguishes the [001] site from the other two. In fact the first order quadrupolar splitting for an axially symmetric EFG depends on the angle of the magnetic field relative to the EFG axis (θ) as

$$\delta\nu \propto 3\cos^2(\theta) - 1\,.$$

So the two large resonances correspond to the [100] and [010] sites with $\theta = 90°$ and the outer lines to the [001] site with $\theta = 0°$.

The results in $SrTiO_3$ indicate that not only can ^{8}Li β-NMR be used as a local magnetic probe, but in some cases it is also sensitive locally to electrostatic fields in solids.

Spin lattice relaxation

In addition to measuring the ^{8}Li resonance, we have measured the spin lattice relaxation. The relaxation is due to coupling of the ^{8}Li to the conduction electrons of the metal (Korringa relaxation) and demonstrates our ability to measure magnetic dynamics.

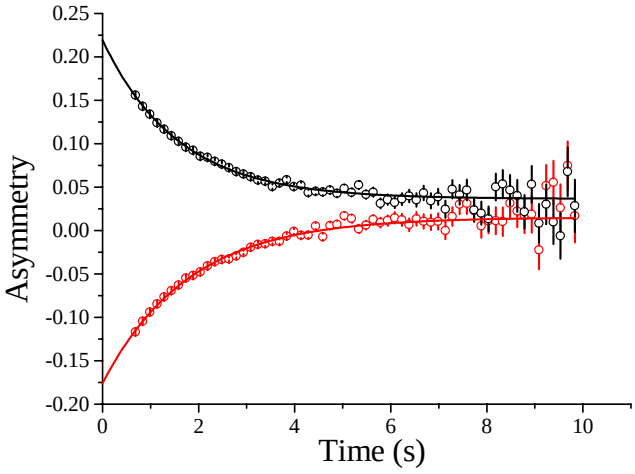

Fig. 79. The spin lattice relaxation of ^{8}Li in Pd. In the experiment the beam was on for the first 0.5 s, then the decay of the asymmetry was monitored.

Experiment 833
Muon spin relaxation studies on MnSi under applied pressure
(I.M. Gat, Columbia)

MnSi is one of the most investigated magnetic systems with itinerant electrons. The compound orders at $T_c = 29.5$ K in a helical magnetic structure with a long period (180 Å). We present μSR studies on a single crystal of MnSi under applied magnetic field and at zero magnetic field under an applied pressure of 8.3 kbar. The measurements confirm the predictions of the self consistent renormalization theory [Moriya, *Spin fluctuations in itinerant electron magnetism*]: close to T_c the relaxation time of muon spins, T_1, is proportional to $T(1-T_c/T)^2$, while at higher temperature T_1 is proportional to $(1-T_c/T)$.

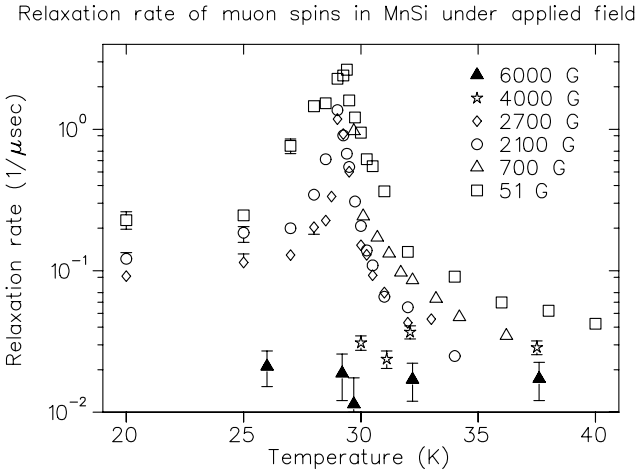

Fig. 80. Temperature dependence of the muon spin relaxation rate $\lambda = 1/T_1$ in MnSi under zero field and applied magnetic fields of 51.5 G, 2115 G, 2700 G, 4000 G and 6000 G. Data under 700 G taken by Dr. Hayano's group [Hayano, *et al.*, J. Phys. Soc. Japan **49**, 1773 (1980)] are plotted for comparison.

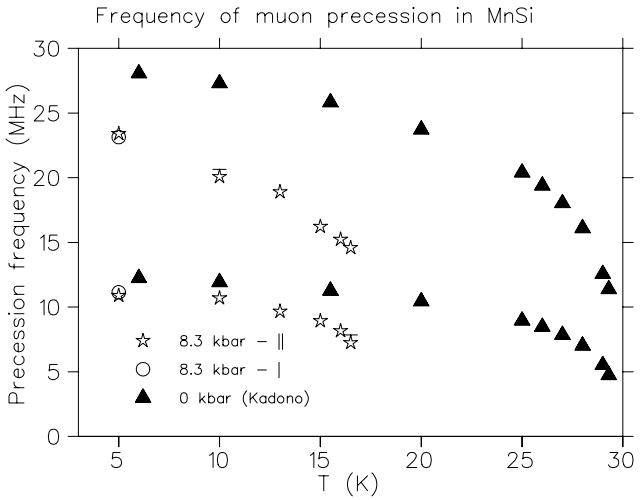

Fig. 81. The muon spin precession frequency in MnSi under an applied pressure of 8.3 kbar. The open circles represent the precession frequencies measured at a previous time. The agreement shows that the pressure didn't change between the times of the measurements. The data are compared with data taken by Dr. Kadono and his collaborators [Kadono, *et al.*, Phys. Rev. **B42**, 6515 (1990)] on MnSi at ambient pressure.

The relaxation time T_1 shows an unexpected field dependence in the paramagnetic phase, for magnetic fields smaller than 3000 G. We propose an explanation for the field dependence of T_1 based on the helical nature of the magnetic structure. A magnetic field of 4000 G completely suppresses the critical spin fluctuations. These findings are in agreement with the magnetic phase diagram of MnSi at ambient pressure (see Figs. 80 and 81).

Experiment 834
μSR study of transverse spin freezing in bond-frustrated magnets
(D.H. Ryan, McGill)

The random addition of antiferromagnetic (AF) exchange interactions to an otherwise ferromagnetic (FM) system leads to a loss of FM order through exchange frustration. In extreme cases, a spin glass (SG) is formed with random isotropic spin freezing and neither net magnetization nor long range order. At lower levels of frustration the system exhibits characteristics of both extremes as long-ranged FM order co-exists with SG order in the plane perpendicular to the FM order. On warming such a system from $T = 0$ K, the SG order first melts at T_{xy} followed by the loss of FM order at T_c. This picture has emerged from mean field calculations, numerical simulations and experimental measurements.

The aim of Expt. 834 is to investigate the magnetic behaviour in the region of T_{xy} in some partially frustrated alloys. Specifically, numerical simulations predict that although the freezing of transverse spin components does not represent a phase transition, it should be accompanied by significant, but non-critical, magnetic fluctuations. Our initial work confirmed the expected signatures of transverse spin freezing could be observed using μSR, however, there was a clear disagreement between the values for T_{xy} determined by μSR and those obtained earlier by applied field Mössbauer spectroscopy. The latter values were systematically lower, by as much as a factor of two in the most extreme case.

Further measurements through 2000 were aimed at understanding this discrepancy. Using a–$Fe_{90-x}Ru_xZr_{10}$ we were able to observe the FM→SG cross-over and also make a direct comparison with T_{xy} values derived from zero-field Mössbauer spectroscopy. A more detailed series of measurements in

the a–Fe_xZr_{100-x} system around $x = 93$ confirmed that the deviation from the applied field Mössbauer values for T_{xy} was a systematic effect. These observations led us to suspect that the ∼3 T field used in the Mössbauer measurements greatly affects both the value of T_{xy} in any given sample, and also changes the critical concentration for the loss of ferromagnetic order.

We have now made two series of runs using Helios to apply fields of up to 5.5 T and measure the effects of an applied field on T_{xy}. The results of our first run using a–$Fe_{92}Zr_8$ are shown in Fig. 82. We were able to observe the fluctuation peak at all fields used and thus followed T_{xy} as the field suppressed it by over a factor of four. This immediately confirms that the applied field is at the origin of the μSR – Mössbauer discrepancy. Theoretical predictions for the functional form of this suppression are limited to mean-field models which predict a dependence of the form:

$$T_{xy}(B) \propto T^0_{xy}\left(1 - \frac{B^p}{A}\right)$$

where A is a constant, and predictions for p range from 2 [Gabay and Toulouse, 1981], 2/3 [Almeida and Thouless, 1978], or 1 [Fischer and Hertz, 1991]. Unfortunately, none of the three predicted forms describes the observed field dependence of T_{xy}. Visual inspection of the trend suggested a $1/B$ dependence (i.e. $p = -1$), in severe disagreement with the predicted forms. The simplest function that reproduced the data, allowed for a scaling of the suppression rate, and gave an asymptotic value of $T_{xy}(\infty) = 0$ was found to be:

$$T_{xy}(B) = T^0_{xy}\left(1 - \frac{B}{(J_s + B)}\right)$$

where the scale factor J_s took a value of 1.5 ± 0.3 T, which is consistent with the 1.36 T saturation polarization of this alloy.

A more extensive series of measurements on four more a–Fe_xZr_{100-x} samples has confirmed that the same functional form for the suppression is observed from the almost ferromagnetic $x = 90$ right through to the spin-glass $x = 93$. Analysis is continuing on this data set.

In a parallel effort, we have developed selective excitation double Mössbauer (SEDM) spectroscopy as a viable probe of dynamics in magnetic materials. We have applied it to the study of the fluctuations at T_{xy} in a–$Fe_{92}Zr_8$ and shown that two independent techniques yield the same fluctuation rates around T_{xy} (see Fig. 83). This agreement, coupled with the nature of the relaxation process detected by SEDM allows us to conclude that moment reversals are the dominant fluctuation in this material around T_{xy}.

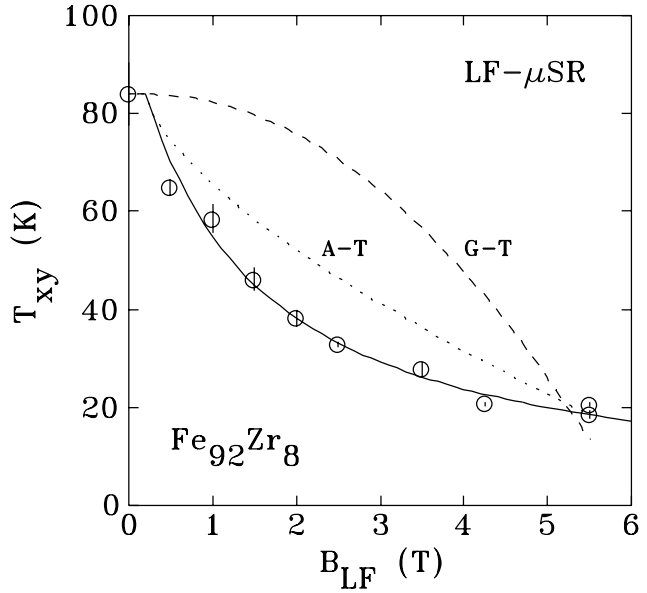

Fig. 82. Field dependence of T_{xy} measured by LF-μSR in a–$Fe_{92}Zr_8$. The solid line is a phenomenological fit described in the text. Dashed (G–T) and dotted (A–T) lines show the mean-field predictions discussed in the text scaled to agree at 0 T and 5 T.

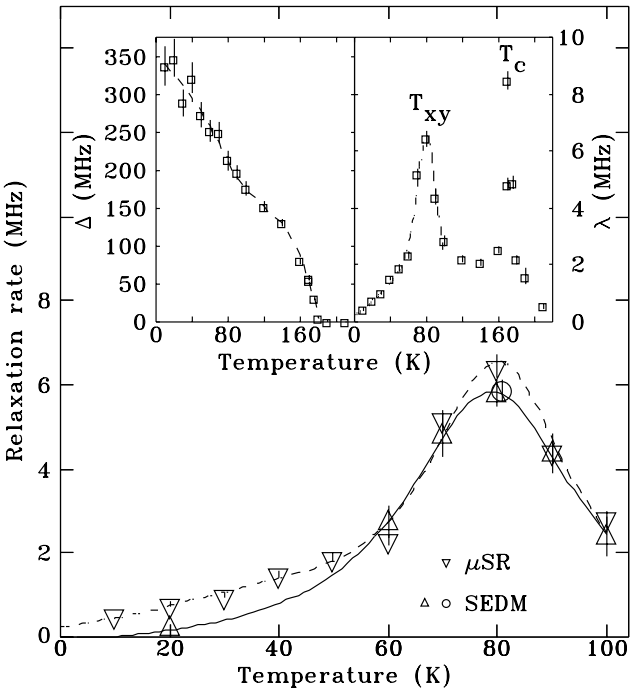

Fig. 83. Inset: Temperature dependence of the static (Δ) and dynamic (λ) relaxation rates in a–$Fe_{92}Zr_8$. Dashed lines are guides to the eye. Body: Relaxation rates from ZF-μSR fits ($\bigtriangledown$) and SEDM fits ($\bigtriangleup$,$\bigcirc$) around T_{xy}. Lines are guides to the eye.

Present status of Expt. 834

We will be continuing this work along two distinct lines.

The first involves tidying up the field shift problem. We have to complete the analysis of the July, 2001 runs so as to determine how the level of frustration affects the rate at which a field suppresses T_{xy}. In parallel with this analysis, we are also extending our Monte Carlo simulation work that led to the prediction of the fluctuation peak at T_{xy}, to include the effects of an external field. In this way we hope to provide some insight into the detailed origins of the field suppression.

The second issue involves addressing a claimed difference between our work on bond frustrated systems, where two, and only two transitions are observed, and a report for a site frustrated material where three distinct transitions have been claimed. Our numerical work shows only evidence for two transitions, as in the bond frustrated case. We expect to clear this up in summer, 2002.

Experiment 835
μSR in doped HfNCl superconductors

(T. Ito, Columbia and CERC)

The layered compounds intercalated ZrNCl and HfNCl (see the inset of Fig. 84) are superconductors with a maximum T_c of ∼15 K and ∼25 K. By the intercalation of alkali metal atoms and organic molecules, carriers are introduced and interlayer distance can be changed. We have performed transverse-field μSR studies on these compounds with magnetic field perpendicular to their layers. The samples were well aligned polycrystals pressed under uniaxial stress. The temperature dependence of the relaxation rate $\sigma(T)$ is shown in Fig. 84. $\sigma(T)$ in the field-cooling process shows a tendency of saturation at low temperatures, characteristic of s-wave superconductors. T_c is not affected by the interlayer distance. T_c as a function of $\sigma(T \to 0)$ is plotted in Fig. 85. $\sigma(T \to 0)$ of superconducting Hf(Zr)NCl is much smaller than that of conventional superconductors such as Nb. With overdoping, in spite of the increase of chemical doping level, superconducting carrier density and T_c decrease, as is observed in the overdoped high-T_c superconductors. We see different tendencies between samples with and without organic molecules, where simple linear correlation is observed for each. We show that T_c is well correlated with $n_{2d,s}/m^*$, where $n_{2d,s}$ is superconducting sheet carrier density. This correlation is common to high-T_c superconductors and quasi-two-dimensional organic superconductors (BEDT-TTF)$_2$Cu(NCS)$_2$, which suggests universal superconducting condensation mechanism among these exotic superconductors.

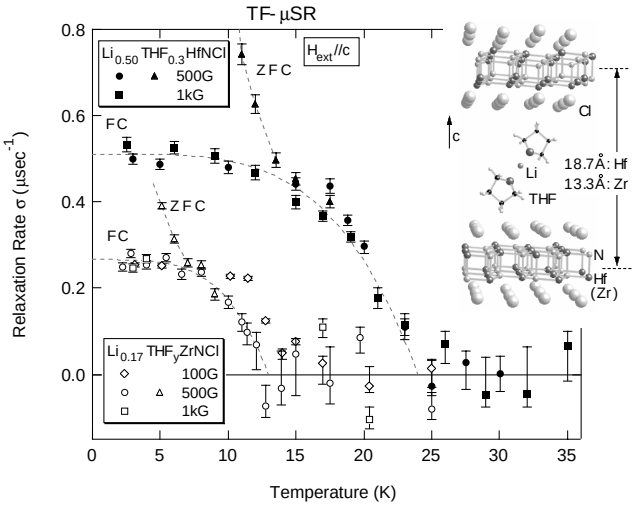

Fig. 84. The temperature dependence of the relaxation rate $\sigma(T)$ in intercalated Hf(Zr)NCl.

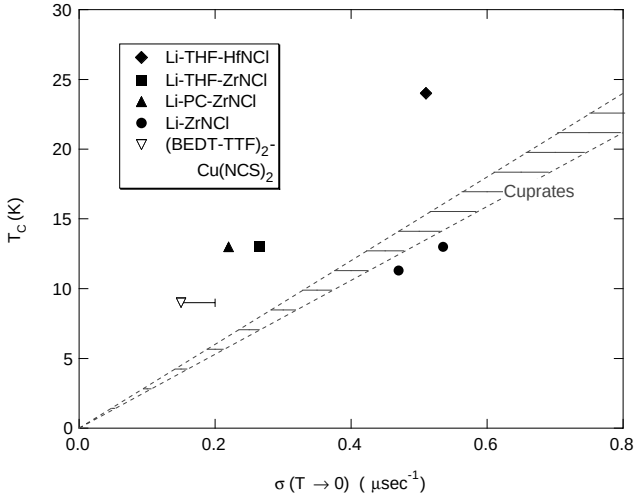

Fig. 85. The correlation between T_c and $\sigma(T \to 0)$ of intercalated Hf(Zr)NCl.

Experiment 842
Mu-substituted free radicals in sub- and supercritical water

(P.W. Percival, SFU)

The beam time used by Expt. 842 during 2001 was split between two projects: formation of muoniated radicals in aqueous solutions of acetone; and kinetics of the reaction between muonium and the formate ion in aqueous solution. In both cases, measurements were made over a wide range of temperature and pressure, from standard to supercritical conditions. Last year's report highlighted muonium kinetics, so the current report is devoted to free radical studies.

It is well established that muonium reacts with acetone as a pure liquid or in solution at "normal" temperatures by addition to the carbonyl oxygen:

$$\mathrm{Mu} + (\mathrm{CH_3})_2\mathrm{CO} \rightarrow (\mathrm{CH_3})_2\dot{\mathrm{C}}\mathrm{OMu}\ .$$

However, in a preliminary investigation of muoniated radicals in supercritical aqueous solutions we found evidence that seemed to contradict this mechanism. Accordingly we carried out the systematic study summarized here.

At temperatures below 250°C the expected radical was detected by transverse field muon spin rotation (μSR). It has a rather low muon hyperfine constant which increases with temperature. At higher temperatures, however, a radical with a much higher hyperfine constant was detected. Examples of the μSR spectra are given in Fig. 86. Hyperfine constants were calculated from the radical precession frequency labelled R_1 and the muon Larmor frequency, corresponding to the large truncated peak in the two spectra of Fig. 86. The results are summarized in Fig. 87.

It is obvious that two different radicals are formed. At low and intermediate temperatures our results are consistent with literature data, denoted by the open symbols in Fig. 87. The small shifts between data sets are consistent with changes in solvent properties for different concentrations of acetone. The question is: What is the identity of the "new" radical found above 250°C?

The key to this riddle is the known keto-enol tautomerism of acetone:

$$(CH_3)_2C{=}O \rightleftharpoons CH_3C(OH){=}CH_2 \ .$$

At low temperature the equilibrium is far to the left, i.e. there is very little of the enol formed. Unlike the usual keto form, the enol has a carbon-carbon double bond instead of the carbon-oxygen double bond. Apparently the equilibrium favours more enol at higher temperatures, since the new radical we have detected is consistent with the 1-muono-2-hydroxypropyl radical, $CH_3\dot{C}(OH)CH_2Mu$, which would be formed by Mu addition to the C=C bond.

Full characterization of this radical is not yet possible, since it requires development of apparatus to perform muon avoided level crossing experiments on samples under the extreme conditions of supercritical water. Nevertheless this work serves to demonstrate the novel chemistry that can be discovered by means of muon studies of such systems.

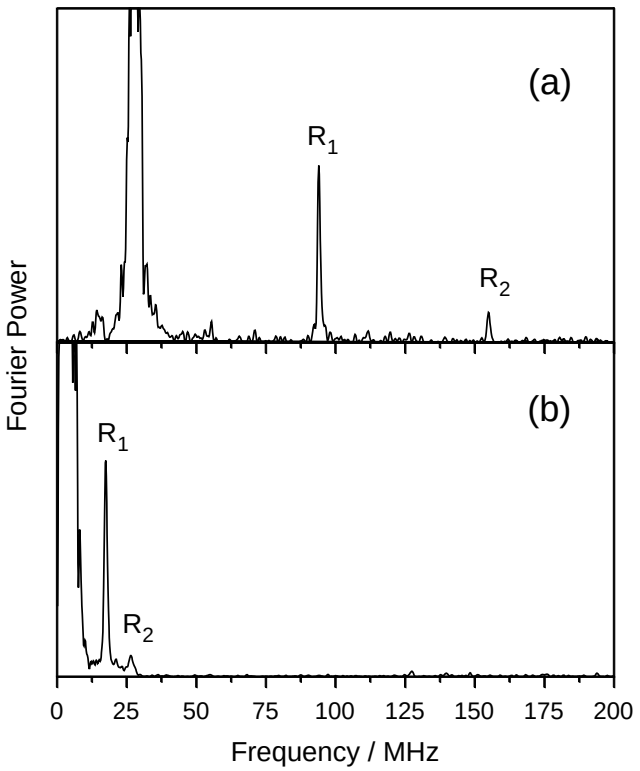

Fig. 86. Muon precession signals from aqueous solutions of acetone at (a) 370°C, 250 bar, 2 kG; (b) 170°C, 190 bar, 320 G. In each case the pair of peaks, denoted R_1 and R_2, is characteristic of a muoniated free radical.

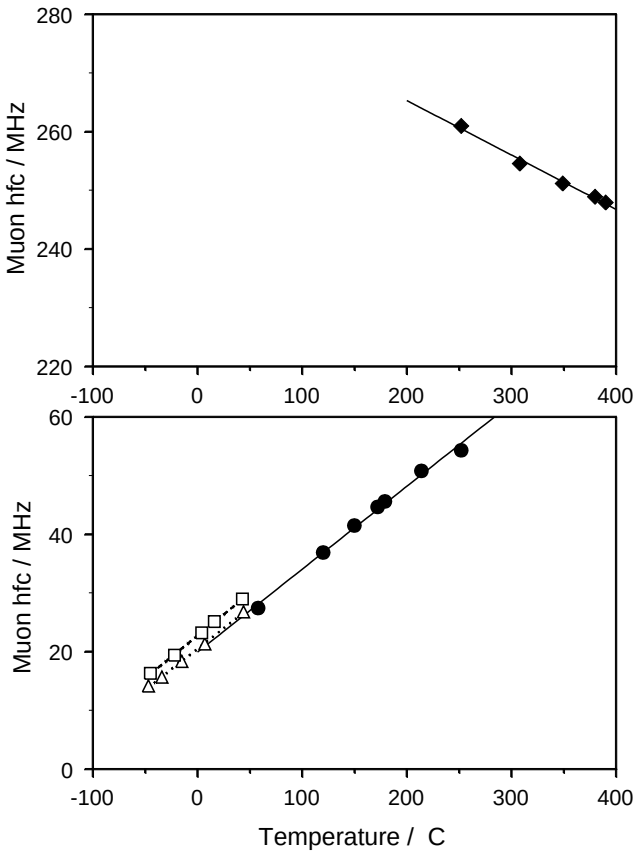

Fig. 87. Muon hyperfine constants for the two radicals detected in aqueous solutions of acetone (filled symbols) compared with literature data (open symbols).

Experiment 846
Complex order parameter symmetry in $YBa_2Cu_3O_{7-\delta}$ at low T and high magnetic field
(J.H. Brewer, UBC; J.E. Sonier, SFU)

Since the spring, 2000 beam period, we have been focused on μSR measurements of UBC grown $YBa_2Cu_3O_{6+x}$ crystals in zero external magnetic field. At the December, 2000 EEC meeting we reported our observation of anomalous weak static magnetism in underdoped ortho-III ($x = 0.67$) and optimally-doped ($x = 0.95$) single crystals. Such weak magnetism had not been observed in early ZF-μSR measurements of the $YBa_2Cu_3O_{6+x}$ system. This was most likely due to a significant background signal in the older measurements. The anomalous weak magnetism we reported seemed to be correlated with the pseudogap crossover T^*. Consequently, we suggested that the result may be consistent with theories predicting the occurrence of spontaneous magnetic fields at temperatures below T^* [Sonier *et al.*, Science **292**, 1692 (2001)]. However, in the past year we have carried out additional measurements on underdoped ($x = 0.80$) and slightly overdoped ($x = 0.985$) crystals. These latest measurements were carried out using the LAMPF spectrometer, but with a side-axis (rather than axial) low-background insert. This experimental modification resulted in a marked improvement in the quality of the ZF-μSR spectra, leading us to identify additional features in the temperature dependence of the muon spin relaxation rate. The results of our most recent study strongly suggest that the weak magnetism we have been observing is in fact associated with spatial inhomogeneity.

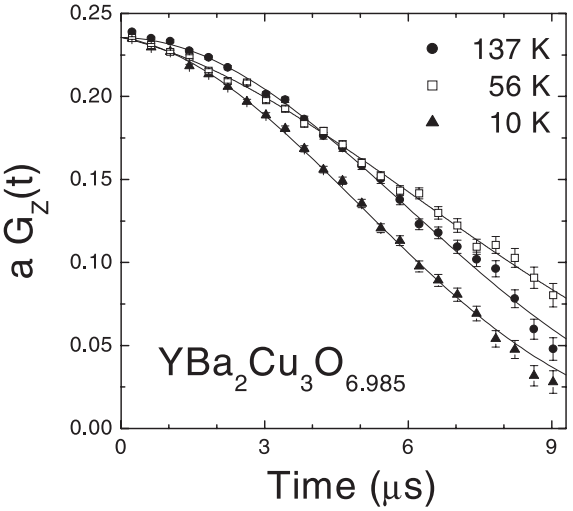

Fig. 88. The time evolution of the muon spin polarization in $YBa_2Cu_3O_{6.985}$ in zero external field at $T = 10$, 56 and 137 K. The signal at 10 K relaxes faster than at 137 K. At 56 K the signal at early times relaxes faster than at 137 K, but exhibits a slower relaxation beyond 5 μs. This latter behaviour indicates a change in the relaxation rate Δ.

In our studies we have found that the ZF-μSR time spectra are well described by a relaxation function that is the product of a static Gaussian Kubo-Toyabe (KT) function and an exponential relaxation function

$$G_Z(t) = [\tfrac{1}{3} + \tfrac{2}{3}(1 - \Delta^2 t^2 \exp(-\tfrac{1}{2}\Delta^2 t^2)] \exp(-\lambda t).$$

The KT function describes the relaxation of the muon spin by the weak nuclear dipole fields. Generally speaking, the relaxation rate, Δ, is not expected to depend on temperature. However, in the overdoped ($x = 0.985$) sample, we find that this assumption leads to poor fits of the time spectra measured near 55 K. Near this temperature we observe a clear change in the ZF-μSR signal (see Fig. 88) that can be accounted for by allowing Δ to vary freely with temperature.

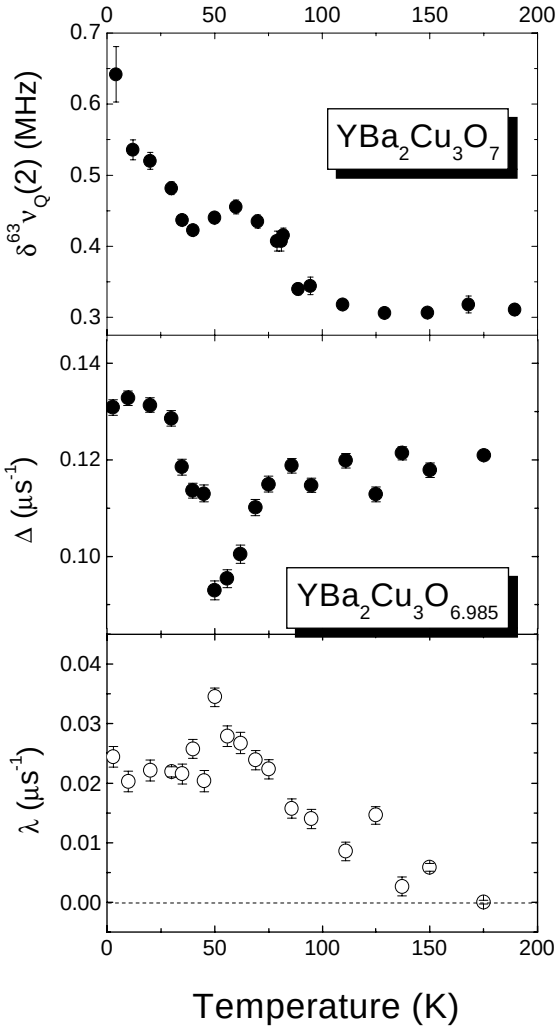

Fig. 89. Top panel: full width at half maximum of the ^{63}Cu(2) NQR line in slightly overdoped $YBa_2Cu_3O_{7-\delta}$ [from Grévin *et al.*, Phys. Rev. Lett. **84**, 1636 (2000)]. Middle and bottom panels: temperature dependence of the Gaussian relaxation rate Δ and the exponential relaxation rate λ in $YBa_2Cu_3O_{6.985}$ from ZF measurements taken with the initial muon spin polarization $P_\mu(0)$ perpendicular to the c-axis of the crystal.

The resulting temperature dependence of Δ shows several features, most notably a large dip near 55 K and a subsequent increase with decreasing temperature below 35 K (see Fig. 89). The latter behaviour was previously observed in the $x = 0.95$ sample, but mistakenly attributed to a change in the exponential relaxation rate λ. As seen in Fig. 89, λ which arises from the weak magnetism of unknown origin, begins to increase below ≈130 K. What is most interesting is that all of these features occur at temperatures where NQR measurements have observed changes in the spatial distribution of charge in the CuO_2 layers of $x \approx 1.0$ samples [Grévin *et al.*, Phys. Rev. Lett. **85**, 1310 (2000)]. Futhermore, several groups have reported local structural changes occurring in $YBa_2Cu_3O_{6+x}$ samples near $T \approx 35$ K, 60 K and 120 K. In our most recent paper submitted for publication, we hypothesize that the weak magnetism associated with λ originates from hole depleted regions of the sample, and the noted features arise from a strong coupling of the charge, spin and lattice degrees of freedom. Given the very different nature of the experiments and the different samples investigated, we have concluded that these effects are an intrinsic property of $YBa_2Cu_3O_{6+x}$, and local structural changes likely occur near $T \approx 35$ K, 60 K and 120 K for a wide range of hole concentrations.

Results of ZF-μSR measurements on underdoped samples performed over the past year show that the local minimum in Δ near $T \approx 55$ K and the increase of Δ at temperatures below 35 K become less pronounced with decreasing x. While the reduction in the size of these features may be related to changes in the μ^+ site(s) and/or increase in mass anisotropy, the CuO chain layers are a more likely cause. It has been suggested that the charge inhomogeneity observed in the CuO_2 planes with NQR is induced by charge ordering in the CuO chain layers. Consequently, the $T \approx 35$ K and $T \approx 55$ K features are strongest for $x = 1.0$, where the chains are completely full.

Experiment 847
Electron-doped high-T_c superconductors
(J.E. Sonier, SFU; G.M. Luke, McMaster)

We have been studying the temperature dependence of the magnetic penetration depth λ_{ab} in the vortex state of the electron-doped high temperature superconductor $Pr_{2-x}Ce_xCuO_4$. These measurements are unique in that they probe the superfluid density in the bulk of the sample. Although the family of electron-doped copper oxide superconductor was discovered in 1989, single crystals of $Pr_{2-x}Ce_xCuO_4$ have only recently become available for μSR studies. The $Pr_{2-x}Ce_xCuO_4$ system is of particular experimental interest because there is no large paramagnetic contribution from the rare earth ion (unlike the more widely studied $Nd_{2-x}Ce_xCuO_4$ system) to influence measurements of λ_{ab}. Besides studying the behaviour of λ_{ab}, we have also been investigating the magnetism in the $Pr_{2-x}Ce_xCuO_4$ system. Such studies are aimed at determining the role of magnetism in electron-doped high-T_c superconductivity and developing a complete generic phase diagram for these systems. Thus far, our studies in Expt. 847 have produced two important findings.

First, we have successfully extracted the in-plane magnetic penetration depth λ_{ab} from measurements of the internal magnetic field distribution in the vortex state of a $Pr_{2-x}Ce_xCuO_4$ single crystal. This is a major achievement given the small size of the samples available to us, and the added complication of magnetism in the material. At low magnetic field ($H = 90$ G) we observed the asymmetric μSR line shape characteristic of a vortex lattice. The magnetic penetration depth λ_{ab} and the additional broadening of the internal field distribution (due primarily to the presence of magnetic moments) were easily determined from fits of the spectra in the time domain. The results (Fig. 90) show that the temperature dependence of λ_{ab} found in the bulk of $Pr_{2-x}Ce_xCuO_4$ single crystals is consistent with conventional s-wave superconductivity. This behaviour is qualitatively similar to that observed in the Meissner state by some of the other groups using surface-sensitive techniques. Thus the failure to observe a clear signature of d-wave pairing symmetry in these other magnetic penetration depth experiments on electron-doped high-T_c superconductors cannot be ascribed to problems with the surfaces of these materials.

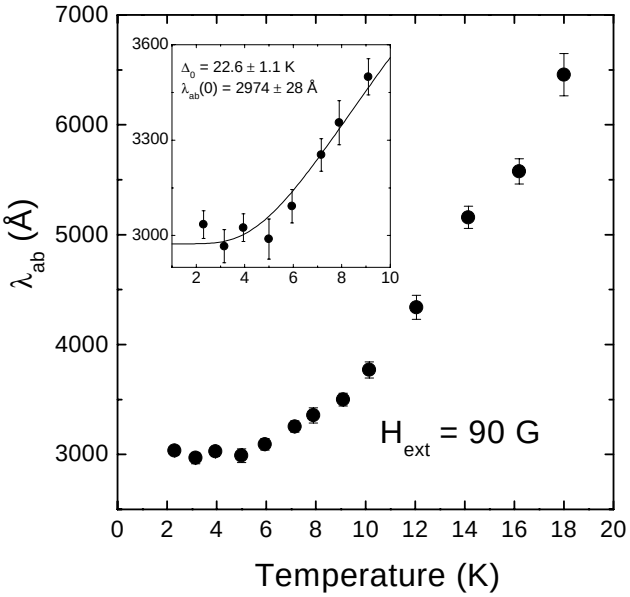

Fig. 90. Temperature dependence of λ_{ab} in the vortex state of a $Pr_{2-x}Ce_xCuO_4$ ($x \approx 0.15$) single crystal. The inset shows a fit for $T \leq 9$ K to the BCS relation (solid curve).

Second, we have established that the superconducting phase of $Pr_{2-x}Ce_xCuO_4$ contains sizeable magnetic moments that are inhomogeneously distributed in the sample. Figure 91 shows fits of the zero-field μSR time spectra to a stretched exponential relaxation function $G_z(t) = \exp[-(\Lambda t)^\beta]$, where Λ is the relaxation rate and β is the power. Measurements in a longitudinal field confirm that the internal magnetic fields are static. At the lowest and highest temperatures we find that $\beta \approx 1$, which is characteristic of dilute static magnetism. We associate the maximum that occurs near 50 K with a reorientation of the Cu spins, which has been previously observed in the parent compound Pr_2CuO_4 by neutrons at high pressure. While we observe no long-range magnetic order (i.e. no coherent precession signal) in zero-external magnetic field, the sensitivity to the Cu-spin reorientation implies that there is some sort of short-ranged magnetic order. We are planning further studies of $Pr_{2-x}Ce_xCuO_4$ to determine the precise origin of the internal magnetism that we have detected.

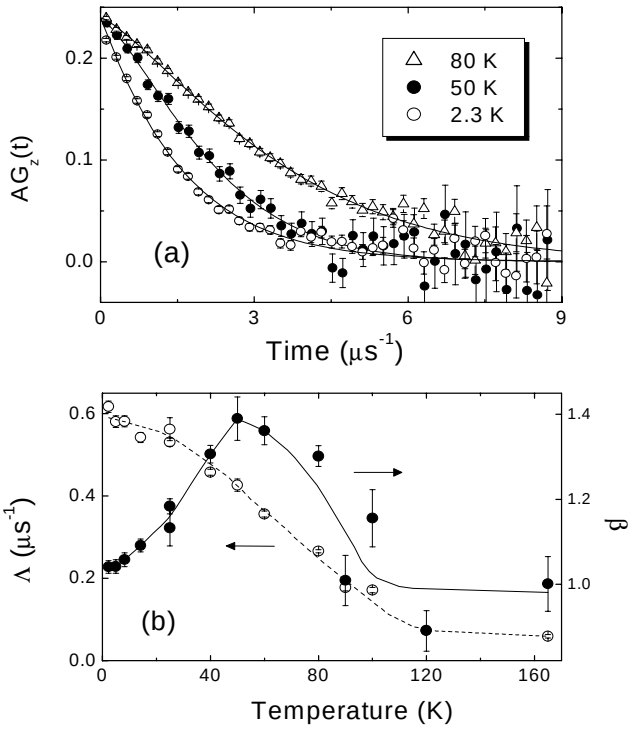

Fig. 91. Top panel: time evolution of the muon spin polarization in a superconducting $Pr_{2-x}Ce_xCuO_4$ crystal for zero-external magnetic field. Bottom panel: results from fits of the zero-field μSR time spectra to a stretched-exponential relaxation function $G_z(t) = \exp[-(\Lambda t)^\beta]$.

Experiment 848
Vortex state of *d*-wave superconductors investigated by muon spin rotation
(R. Kiefl, R. Miller, UBC/TRIUMF)

Static fields in vortex cores of $YBCO_{6.50}$

Evidence for static fields induced in the vortex cores of ortho-II YBCO have been reported in previous Expt. 848 reports. The results are in press [Miller *et al.*, Phys. Rev. Lett. **88**].

Single transition to AF and SC groundstate in $YBCO_{6.35}$

Transverse field and zero field μSR relaxation/rotation measurements in ortho-II $YBCO_{6.35}$ have revealed a single transition at $T = 13.8$ K to a superconducting (SC) and antiferromagnetic (AF) state. Figure 92(a) shows the magnetization in $YBCO_{6.35}$ measured in a small field. The sharp transition at $T = 13.8$ K is good evidence for a bulk superconductor. Figure 92(b) shows the temperature dependence of the main frequency measured in zero field

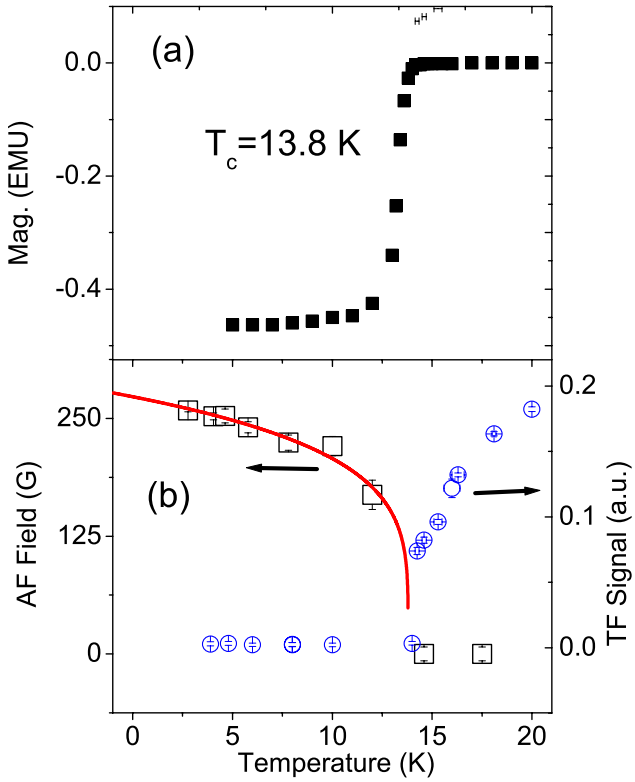

Fig. 92. Panel (a) temperature dependence of the magnetization in $YBCO_{6.35}$ in a small field. A sharp superconducting transition is seen at $T = 13.8$ K. Panel (b) (Left-hand scale) Magnetic field at a muon site below T_N. The low temperature value is approximately 90% of the field found in the parent YBCO compound. (Right-hand scale) Long-time asymmetry of the transverse field muon polarization signal, showing a transition near T_N to a 100% antiferromagnetic state.

(left-hand scale). The zero temperature frequency is approximately 90% of the frequency seen in the parent compound $YBCO_{6.0}$. The right-hand scale seen in Fig. 92(b) shows the temperature dependence of the long-time μSR polarization asymmetry. The decrease in the asymmetry at T_N shows that the entire sample undergoes the transition to an AF state.

This finding is unusual in that previous reports of coexistent T_N and T_c, found in the LSCO family of superconductors, have pockets of antiferromagnetism surrounded by superconductivity, e.g. the AF nature of the low temperature ground state is not homogeneous. In $YBCO_{6.35}$, it appears that all muons stop near large internal fields. The rapid damping of the zero field signal, however, seems to indicate that field distribution around the muon site(s) is large. The antiferromagnetism is quite disordered.

This work is currently under preparation for publication. The data are discussed in terms of stripes and cluster spin glasses.

Future plans

We plan to run a large single crystal of $YBCO_{6.50}$ in Belle in August to see if we can reproduce the signals from vortex core fields. This sample was used in a neutron scattering study that revealed no sharp peak at the AF wave vector after the application of a field, indicating that any vortex core antiferromagnetism must be spatially disordered in these crystals. Further, we intend to use OMNI to measure a slightly higher doped YBCO than in $YBCO_{6.35}$, and see if we can measure the SC transition at higher temperatures and see the AF transition at lower temperatures.

Experiment 849
Spin structure and magnetic volume fraction of La214 systems
(Y.J. Uemura, Columbia; K.M. Kojima, Tokyo)

Last year we reported that we found incommensurate spin density wave ordering in $La_2CuO_{4.11}$ and $La_{1.88}Sr_{0.12}CuO_4$. The amplitude of oscillations was less than expected from weak transverse field measurements, so we concluded that only a fraction of the sample is magnetically ordered.

More data and a careful analysis of the experimental results allowed us to extract some useful information.

We found unusual behaviour for the magnetic order parameter. To illustrate this, Fig. 93 shows the spectra for $La_2CuO_{4.11}$ (LCO:4.11) and antiferromagnetic La_2CuO_4 (AF-LCO). For conventional systems like AF-LCO, the amplitude of oscillations is nearly temperature independent, but frequency increases with decreasing temperature. In contrast, LCO:4.11 shows

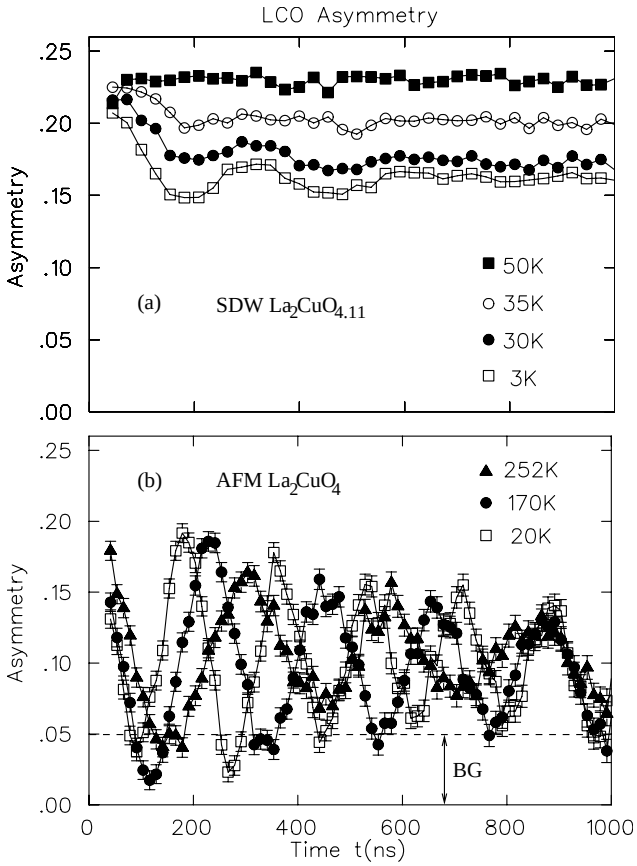

Fig. 93. Comparison between ZF-μSR spectra of $La_2CuO_{4.11}$ and antiferromagnetic La_2CuO_4.

an increased amplitude of oscillations as we lower the temperature, but frequency remains almost constant.

In order to elucidate this behaviour, a simple model was proposed. Magnetic ordering exists only in a certain fraction of the crystal. Computer simulations were performed for different configurations of regions with static magnetism. These can be seen in the inset of Fig. 94.

In order to decide which model best describes the experimental results, we looked at the fraction of muon sites that have a non-zero magnetic field and at the signal that one gets for this distribution.

The "sandwich model" contains completely ordered Cu planes. The resulting signal has a long lived Bessel-like oscillation, with little decay of non-relaxing signal, which does not fit experimental results well.

The "island model" contains circular regions with magnetic ordering. A density of 30% of the spins showing static magnetism gives a fraction of 40% of muon sites with non-zero magnetic field (as in the measured data for LCO:4.11). The relaxation of the oscillating signal is also a measure of the size of the "island", which we estimate to be 15–30 Å.

A correlation of spin orientation in overlapping magnetic regions in neighbouring planes is a possible

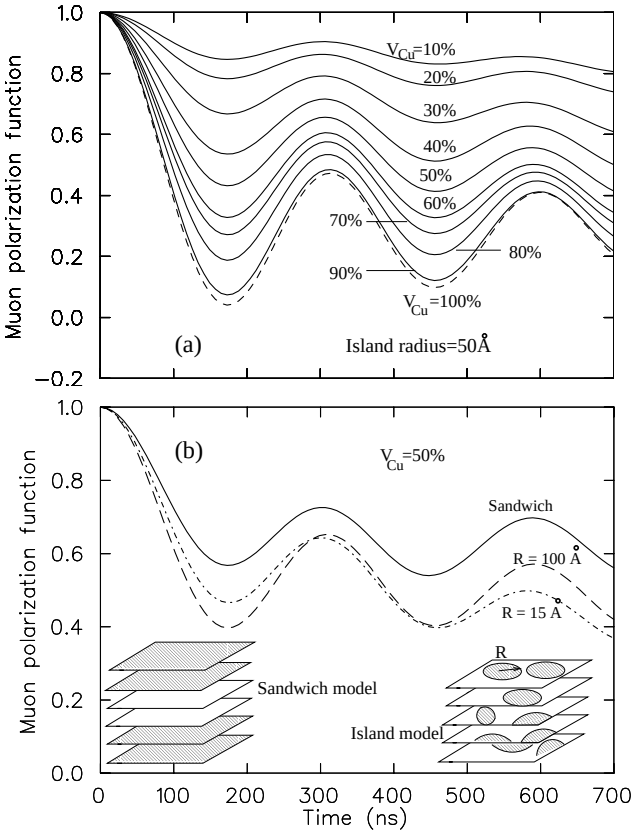

Fig. 94. Computer simulation results for different magnetic configurations.

explanation for the long range order, observed by neutron scattering.

In transverse magnetic field μSR measurements, sensitive to the in-plane magnetic field penetration depth λ_{ab}, the results for LCO:4.11 and LSCO:0.12 follow correlations found for underdoped, overdoped and Zn-doped HTSC systems in a plot of T_c versus the superconducting relaxation rate $\sigma(T \rightarrow 0)$. This indicates that the volume-integrated value of n_s/m^* (superconducting carrier density/effective mass) is a determining factor for T_c, not only in HTSC systems without static magnetism, but also in the present systems where superconductivity co-exists with static SDW spin order.

We have performed zero-field and transverse-field μSR of $La_{1.85-y}Eu_ySr_{0.15}CuO_4$, where Eu doping stabilizes the "stripe" structures in the spin and charge degrees of freedom. In Fig. 95a, zero-field μSR spectra are shown for Eu concentrations $y = 0.05, 0.1$ and 0.2. The magnetic volume fraction, which is indicated by the amplitude of the precession in the $t < 0.3$ μs time range, increases as the Eu doping proceeds. The size of the ordered moments, as shown by precession frequencies, is independent to the Eu concentration, and is common to the frequency in the 1/8 carrier doping, where stripes are fully stabilized. These results

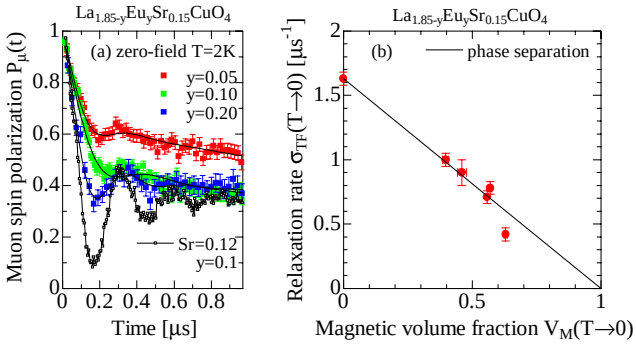

Fig. 95. (a) zero-field μSR of $La_{1.85-y}Eu_ySr_{0.15}CuO_4$. (b) Superfluid density vs. magnetic volume fraction.

indicate that the static magnetism exhibits a *partial volume fraction*, with area covered by islands of ordered moments increasing as Eu doping proceeds, without changing the size of the ordered moments.

From transverse-field μSR, the superfluid density was estimated, and shown in Fig. 95b, as a function of the static magnetic volume fraction. There is a tradeoff between the magnetic volume fraction (V_M) and the superfluid density $n_s/m^* \propto \sigma_{\rm TF}$. This suggests a phase separation between the magnetism and superconductivity. The solid line in Fig. 95b indicates a model where superfluidity originates only from the non-magnetic volumes. The results are interpreted in the context of the recent discoveries of microscopic phase separations between the superconducting phase and other phases.

Experiment 852

Magnetic phases in geometrically frustrated rare earth pyrochlores

(S. Dunsiger, LANL; J. Gardner, NRC; R. Kiefl, UBC)

In systems where magnetic ions occupy the vertices of edge or corner sharing triangular units, the combination of the strength and sign of the interactions and local anisotropy may give rise to situations where there is no spin configuration which simultaneously satifies all the magnetic couplings. Stacked triangular, kagomé, fcc, and pyrochlore lattices are all examples of such *geometric* frustration. The purpose of Expt. 852 is to apply μSR to further our understanding of the effect of this frustration on the ground state and low lying magnetic excitations in the pyrochlores $A_2B_2O_7$, where magnetic ions form a network of corner sharing tetrahedra. Unlike many other systems having geometric frustration, pyrochlores are noted for their high degree of chemical order, which is important for minimizing effects due to disorder.

Geometric frustration leads to the formation of a wide range of exotic ground states. A vast body of work has been carried out on 3*d* and 4*d* transition metal pyrochlores. These are generally insulators where novel

properties such as cooperative paramagnetism [Gardner *et al.*, Phys. Rev. Lett. **82**, 1012 (1999)] partial, non-collinear antiferromagnetic ordering [Raju *et al.*, Phys. Rev. **B59**, 14489 (1999); Champion *et al.*, Phys. Rev. **B64**, 140407(R) (2001)], spin-freezing [see, for instance Raju *et al.*, Phys. Rev. **B46**, 5405 (1992); Gingras *et al.*, Phys. Rev. Lett. **78**, 947, (1997)], and dipolar "spin-ice" behaviour [Harris *et al.*, Phys. Rev. Lett. **79**, 2554 (1997); Harris *et al.*, Phys. Rev. Lett. **81**, 4496 (1998); Bramwell and Harris, J. Phys. Cond. Matter **10**, L215 (1998); Ramirez *et al.*, Nature **399**, 333 (1999); Siddharthan *et al.*, Phys. Rev. Lett. **83**, 1854 (1999)] have been observed. There has, however, been growing interest in the interplay between itinerant and local moments in geometrically frustrated systems. The 5*d* transition metal pyrochlores are mainly metallic, resulting from the extended nature of the 5*d* orbitals. Despite the large number of transition metal compounds which crystallize in the pyrochlore structure and the wide range of physical phenomena observed in these materials, superconductivity had not been observed until the recent discovery of bulk superconductivity in the 5*d* pyrochlore, $Cd_2Re_2O_7$ [Sakai *et al.*, J. Phys. Cond. Matter **13**, L785 (2001); Hanawa *et al.*, Phys. Rev. Lett. **87**, 187001 (2001)].

Recent investigations [Sakai *et al., op. cit.*; Hanawa *et al., op. cit.*; Jin *et al.*, Phys. Rev. **B64**, 180503(R) (2001); Jin *et al.*, cond-mat/0108402 (2001); Hanawa *et al.*, cond-mat/0109050 (2001)] have demonstrated the existence of two phase transitions in this compound. The first, occurring at a temperature of about 200 K, is a continuous structural transition which is accompanied by drastic changes in resistivity and magnetic susceptibility. On further lowering the temperature, $Cd_2Re_2O_7$ has been shown to exhibit bulk superconductivity below a sample dependent transition temperature of about 1 K [Sakai *et al., op. cit.*; Hanawa *et al.*, Phys. Rev. Lett. **87**, 187001 (2001); Jin *et al.*, Phys. Rev. **B64**, 180503(R) (2001)]. Preliminary measurements in the superconducting state indicate that $Cd_2Re_2O_7$ is a type-II superconductor with H_{c1} less than 0.002 T and estimates of the upper critical field, H_{c2}, ranging from 0.2 T to 1 T. None of the measurements reported to date extend below 0.3 K ($T/T_c \sim 0.3$). We report the first measurements on $Cd_2Re_2O_7$ below 300 mK, temperatures which are necessary (for $T_c \sim 1$ K) to extract information about the superconducting order parameter symmetry. In July, 2000 we performed transverse field (TF) and zero field (ZF) muon spin rotation (μSR) measurements on single crystal samples of $Cd_2Re_2O_7$ in an Oxford Instruments dilution refrigerator on the M15 beam line at TRIUMF. The crystals were mounted such that the cubic (100) direction would be parallel to the applied magnetic field direction. The ZF-μSR measurements reveal very small internal magnetic fields which are characteristic of nuclear dipoles, indicating no significant electronic magnetism either above or below T_c. The TF-μSR results provide the first measurement of the internal field distribution in the vortex state in this material. In particular, temperature dependent studies from 20 mK to 4 K indicate a penetration depth which levels off as $T \to 0$, suggestive of a fully gapped Fermi surface with a rather large zero temperature value of the penetration depth, $\lambda(0) \sim 7500$ Å.

Figures 96(a) and (b) show typical μSR spectra in a transverse field of 0.007 T, for temperatures above and below T_c respectively. Examination of these data clearly shows an enhanced depolarization rate on entering the superconducting state resulting from the inhomogeneous field distribution associated with the flux line lattice. This represents the first experimental observation of the vortex lattice in $Cd_2Re_2O_7$ and

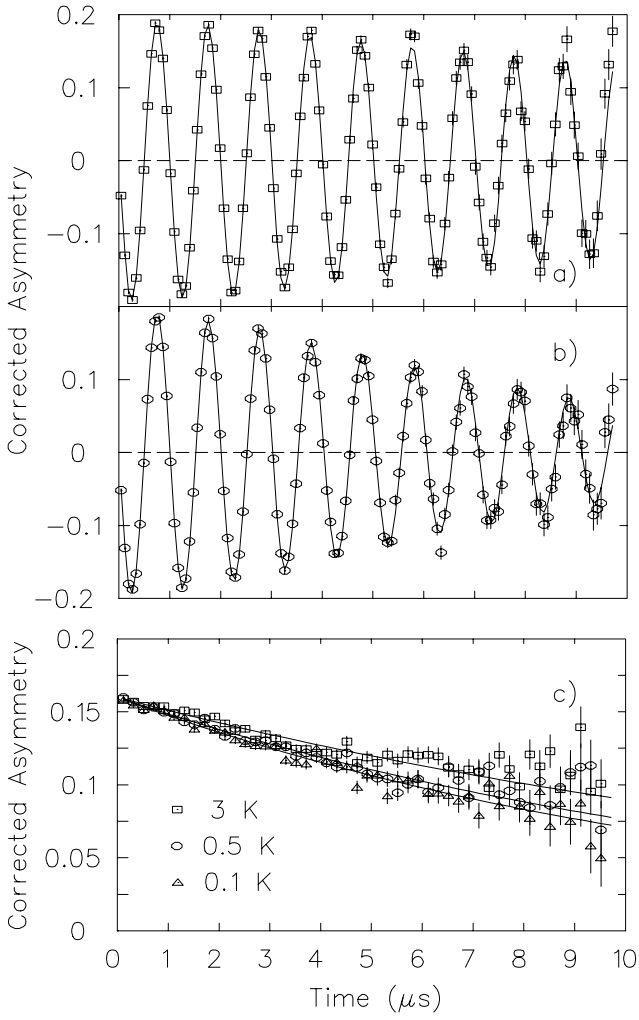

Fig. 96. Typical μSR spectra in $Cd_2Re_2O_7$ obtained in a transverse magnetic field of 0.007 T at temperatures of (a) T=1.5 K (above T_c) and (b) T=100 mK (below T_c). (c) Zero field spectra in $Cd_2Re_2O_7$ at various temperatures.

provides clear evidence that this material is a type-II superconductor. The observed increase in the TF line broadening below T_c can be attributed entirely to the vortex lattice since the ZF muon spin relaxation rate was small and roughly temperature independent below 2 K. Zero field measurements indicate no significant electronic magnetism in this superconductor, suggesting that magnetic frustration does not play a direct role in the superconductivity.

Following the work of Sonier *et al.* [Rev. Mod. Phys. **72**, 769 (2000) and references therein], a Ginzburg-Landau (GL) model has been applied to the magnetic field distribution for the single crystal. In GL theory, the size of the vortex core is determined by the applied magnetic field, H, and the GL coherence length normal to the applied field, $\xi_{\rm GL}$, while the penetration depth provides the length scale of the decay of magnetic field away from the vortex core. The field distribution is calculated from the spatial distribution of magnetic field [Yaouanc *et al.*, Phys. Rev. **B55**, 11107 (1997)],

$$B(\mathbf{r}) = \frac{\Phi_0}{S}(1-b^4)\sum_{\mathbf{G}} e^{-i\mathbf{G}\cdot\mathbf{r}}\frac{uK_1(u)}{1+\lambda^2 G^2}, \qquad (1)$$

where $u^2 = 2\xi_{\rm GL}^2 G^2(1+b^4)[1-2b(1-b^2)]$, $K_1(u)$ is a modified Bessel function, $\mathbf{G}$ is a reciprocal lattice vector of the vortex lattice, $b = H/H_{c2}$ is the reduced field, Φ_0 is the flux quantum and S is the area of the reduced unit cell for a hexagonal vortex lattice.

As can be seen from Eq. 1, the field distribution depends on both the penetration depth and GL coherence depth. The GL coherence length can be obtained from the known value of the upper critical field using the expression $\xi_{\rm GL} = (\Phi_0/2\pi H_{c2})^{1/2}$ where Φ_0 is the flux quantum. A range of values for H_{c2} has been reported and consequently, to provide a self-consistent measurement of λ, the field dependence of the linewidth was measured. To account for any possible instrumental field dependence in the linewidth, measurements were made above the transition temperature (2 K) at each field value after which the sample was field-cooled to 100 mK. The measured linewidth in the normal state was subtracted in quadrature from that observed at 100 mK and the results are plotted in Fig. 98 as a function of applied magnetic field. As can be clearly seen, the linewidth decreases almost linearly with applied field. This is attributed to the linear increase in the volume taken up by the vortices. The linewidth parameter, σ_{FC}, approaches zero at a field of 0.5 T which is our estimate of $H_{c2}(\mathrm{T}\rightarrow 0)$ and is consistent with measurements on other samples. This estimate of the critical field corresponds to $\xi_{\rm GL} \sim 260$ Å. Using this value, we obtain the penetration depth using the field distribution shown in Eq. 1. The resulting temperature dependent penetration depth is shown in Fig. 99.

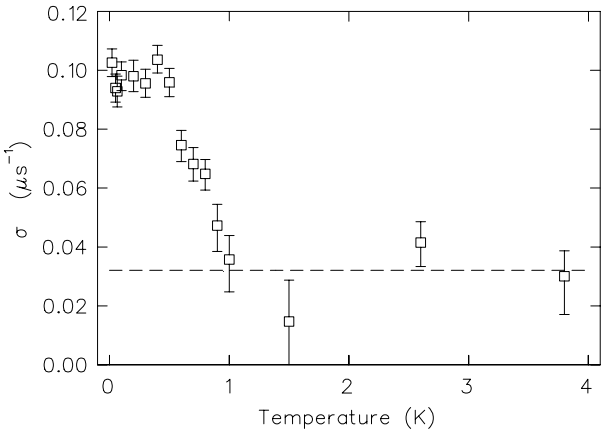

Fig. 97. Linewidth parameter σ as a function of temperature in a transverse magnetic field of 0.007 T applied along the (100) direction.

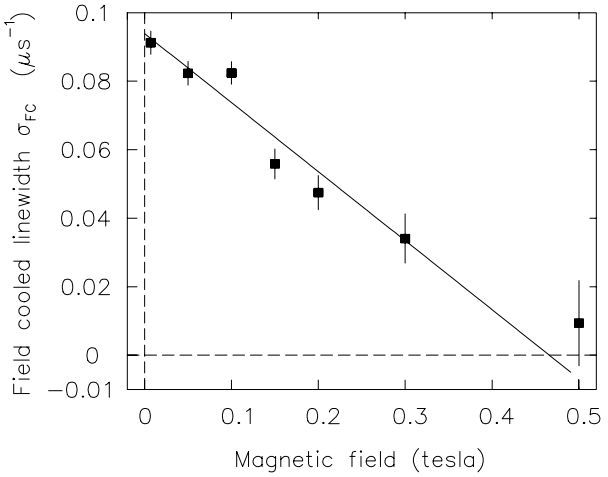

Fig. 98. Linewidth parameter σ_{FC} as a function of magnetic field applied along the (100) direction. The normal state contribution has been subtracted as described in the text. Measurements were taken at a temperature of 100 mK.

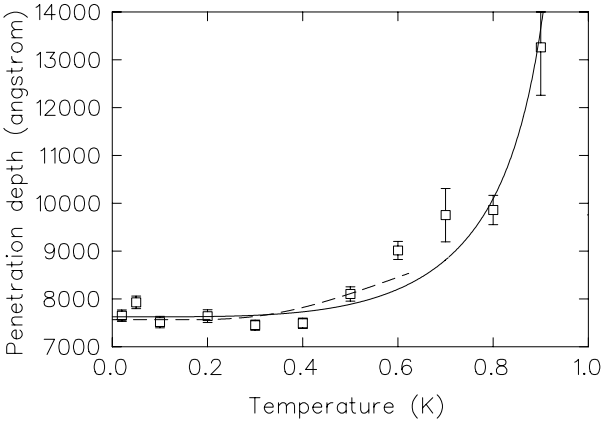

Fig. 99. Penetration depth as a function of temperature in a magnetic field of 0.007 T applied parallel to the (100) direction. The solid and dashed lines are fits to Eqs. 2 and 3 respectively.

As expected from the small values of linewidth, at the base temperature we observe a rather large value of the penetration depth, $\lambda(0) \sim 7500$ Å. We note that this value of penetration depth is significantly larger than most oxide superconductors where values ranging from 1000–2000 Å are typical [Uemura *et al.*, Phys. Rev. Lett. **66**, 2665 (1991); Aegerter *et al.*, J. Phys. Cond. Matt. **10**, 7445 (1998)].

As the penetration depth is related to the concentration of superconducting carriers, its temperature dependence is a measure of the low-lying electronic excitations. As such, the presence of a nodeless superconducting energy gap is indicated by a leveling off of the penetration depth as the temperature decreases below T_c. As is clearly seen in Figs. 97 and 99, the linewidth and penetration depth respectively become temperature independent as the temperature decreases below about 0.4 K, consistent with a fully gapped Fermi surface. Consequently, we conclude that the superconducting order parameter in $Cd_2Re_2O_7$ is consistent with a nodeless energy gap suggesting either s-wave symmetry or exotic pairing symmetries, such as p-wave, which can also exhibit a fully gapped Fermi surface. For comparison, the solid line in Fig. 99 represents fits to the two fluid approximation

$$\frac{\lambda^2(0)}{\lambda^2(T)} = [1 - (T/T_c)^4], \qquad (2)$$

while the dashed line is a fit to the BCS temperature dependence

$$\lambda(T) = \lambda(0)\left[1 + \sqrt{\frac{\pi\Delta_0}{2T}}\exp\left(\frac{-\Delta_0}{T}\right)\right] \qquad (3)$$

where $\Delta_0 = 1.74(11)$ K.

The London penetration depth, λ, provides a direct measure of the ratio of superconducting carrier concentration to effective mass, n_s/m^*,

$$\frac{1}{\lambda^2} = \frac{4\pi n_s e^2}{m^* c^2}\left(1 + \frac{\xi_0}{l}\right)^{-1}, \qquad (4)$$

where ξ_0 is the Pippard coherence length, and l is the mean-free path. There is considerable uncertainty in estimates of the mean-free path with reported values ranging from 200–700 Å [Jin *et al.*, Phys. Rev. **B64**, 180503(R) (2001); Hiroi and Hanawa, cond-mat/0111126 (2001)] and it is unclear whether $Cd_2Re_2O_7$ is a superconductor in the clean or dirty limit. Under the assumption of a clean superconductor, such that $\xi_0/l \ll 1$, a value of $n_s m_e/m^*$ of 5.0×10^{25} m^{-3} can be obtained using Eq. 4 and the measured penetration depth. It is important to note that this quantity depends strongly on the clean-limit assumption and a value of $l \sim$200 Å leads to a dirty limit superconductor with $\xi_0 \sim$470 Å and $n_s m_e/m^* \sim 1.4 \times 10^{26}$ m^{-3}. Clearly, precise determination of the mean free path for $Cd_2Re_2O_7$ is needed to allow accurate quantitative information to be extracted. If the material is in the clean limit, the present results provide strong evidence for a fully gapped Fermi surface.

Experiment 876
Disordered magnetism near magnetic instabilities in *f*-electron materials
(D.R. Noakes, Virginia State)

The discussion of this experiment in last year's Annual Report described ZF- and LF-μSR measurements of UPdSn and members of the $PrAu_2(Si_{1-x}Ge_x)_2$ alloy series. A short paper comparing the data from UPdSn to earlier data from CeCuSn was presented at the 2001 Strongly Correlated Electron Systems Conference in Ann Arbor, MI, in August, and will appear in the proceedings [Physica B, in press]. This year, additional measurements were made on $U_{0.94}Y_{0.06}CoAl$ and at dilution refrigerator temperatures in $PrAu_2Si_2$.

$U_{0.94}Y_{0.06}CoAl$

Pure UCoAl has no spontaneous magnetic ordering to low temperatures, but a metamagnetic transition in a relatively low applied field of 0.8 T. Andreev *et al.* [J. Magn. & Magn. Mater. **196-197**, 658 (1999)] discovered that alloying small amounts of non-magnetic yttrium on the uranium site causes ferromagnetic ordering to occur. From about 1% Y to 6% Y, the Curie temperature is roughly constant near 15 K, but the 4.2 K bulk ordered moment rises from very small values to near 0.1 μ_B per formula unit (much less than the uranium free-ion moment of 3.2 μ_B). Beyond 6% Y, both T_C and the ordered moment fall back toward zero. Other researchers had already established that there is very little muon spin relaxation in pure UCoAl. In August, we measured μSR in $U_{0.94}Y_{0.06}CoAl$, the composition of strongest ferromagnetism, at M20.

The polycrystalline sample was small, and, mounted on a silver backing, generated a relaxing asymmetry of only 0.055 when the full asymmetry measured in transverse field was 0.23 (the difference is generated by muons that missed the sample and stopped in silver, in which they do not relax in zero or longitudinal field). ZF relaxation was consistent with fields generated by the nuclear moments in the sample, with little, if any, indication of electronic moments, down to 20 K. A fast-relaxing signal consistent with the freezing of dilute electronic moments in the sample begins to appear near 16 K and increases in amplitude until it saturates at $\simeq$0.034 (representing about 60% of the sample volume) at 12 K and below. Figure 100 shows the ZF asymmetry spectrum at 3 K, with the solid line

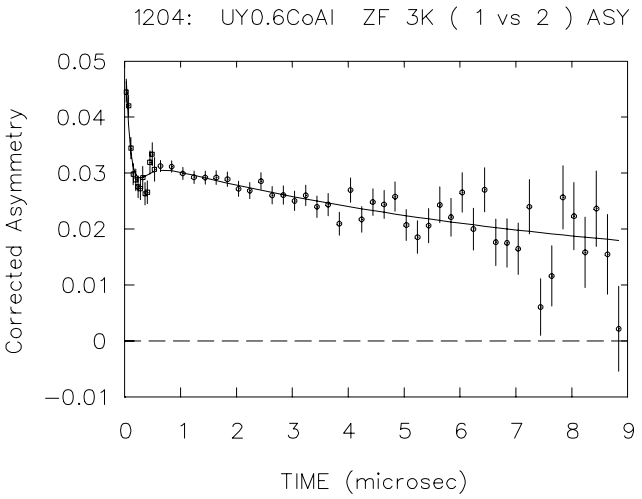

Fig. 100. ZF asymmetry spectrum of $U_{0.94}Y_{0.06}CoAl$ at 3.0 K, with solid line showing the fit of the inhomogeneous-freezing model described in the text.

showing the fit of static Lorentzian Kubo-Toyabe relaxation (the frozen-state signal) plus a slowly-relaxing signal caused primarily by nuclear moments in the portion of the sample that remains paramagnetic. Measurements in longitudinal field support this model.

While static Lorentzian Kubo-Toyabe relaxation is normally associated with the frozen state of dilute-moment spin glasses, this relaxation function is primarily caused by a positionally-disordered distribution of dilute moments, and does not necessarily mean that the moment pointing directions are disordered. I have shown, using numerical simulations published in the Journal of Magnetism and Magnetic Materials, that long-range ferromagnetic order in a polycrystalline, dilute, magnetic alloy produces a ZF muon spin relaxation function that is difficult to distinguish from the standard Lorentzian Kubo-Toyabe. Independently, there are indications of ferromagnetism in our experimental data. When tens of Gauss transverse field are applied below 12 K, sufficient bulk magnetization develops in the sample to cause relaxation of muons that miss the sample, and when that field is removed, the sample has remnant magnetization that continues to affect the polarization of muons that miss the sample.

Our interpretation is that $U_{0.94}Y_{0.06}CoAl$ is a dilute-moment ferromagnet. When yttrium is alloyed onto the uranium site, instead of all the remaining uranium ions each gaining a small moment, no more than one uranium per yttrium ion gains a moment, but each moment created is roughly of Bohr-magneton size. Further, only about 60% of the volume of our sample enters the ferromagnetic state. The other 40% appears to remain paramagnetic.

$PrAu_2Si_2$

Measurements in 2000 on the $PrAu_2(Si_{1-x}Ge_x)_2$ series described in last year's Annual Report were performed in a cryostat with a base temperature near 1.9 K. This was sufficient to allow us to detect ZF coherent oscillations in the antiferromagnetic states of $PrAu_2Ge_2$ and $PrAu_2(Si_{0.8}Ge_{0.2})_2$. In $PrAu_2Si_2$, which is nominally a spin glass with $T_g \approx 3$ K, however, we saw no clear freezing effect down to 1.9 K, and felt that data at dilution-refrigerator temperatures was needed. In 2001, we took advantage of an opportunity to collect a small amount of such data during an unrelated experiment, and found that there is only smooth variation of ZF behaviour with no clear indication of magnetic freezing down to 0.04 K. Thus, in spite of bulk-probe signatures of spin-glass freezing, in μSR, $PrAu_2Si_2$ looks more like a frustrated magnetic system with electronic fluctuations that slow down a bit as temperature is lowered, but never actually freeze. This is an unusual discrepancy with the bulk probe results that we are still trying to understand.

Experiment 883
Muoniated methyl and associated free radicals
(P.W. Percival, SFU)

This is the first progress report on this project, which was first approved in June, 2000. It is a successor to Expt. 749, which applied the muon spin probe to investigate topical and/or fundamental questions in free radical chemistry. The general method for these projects involves addition of muonium (Mu) to an unsaturated molecule such as an alkene or arene, resulting in a free radical incorporating the muon in place of a proton. Such a radical is termed a muoniated radical, to emphasize the formal replacement of a hydrogen atom by muonium in what is otherwise a recognized chemical structure (cf. a deuterated molecule, which contains D instead of H). In terms of electronic structure there is no difference between the H and Mu analogues (at least, to the level of the Born-Oppenheimer approximation). In most respects the muoniated radical behaves like its H analogue and the muon can be viewed as a passive spin probe. However, the low mass of Mu compared to H can result in significant isotope effects, particularly to intramolecular motion.

The specific aim of Expt. 883 is to detect the muoniated methyl radical, $\cdot CH_2Mu$, and study its vibrational motion via measurements of electron-nuclear hyperfine constants as a function of temperature. A previous attempt (TRIUMF Expt. 546) failed to detect $\cdot CH_2Mu$ due to the instability of the precursor, diazomethane (CH_2N_2). However, we did manage to detect and study the trimethylsilyl derivative [Addison-Jones *et al.*, Hyp. Int. **106**, 143 (1997)]. Experiment

883 is based on an alternative strategy, using ketene as the radical precursor:

$$\mathrm{Mu} + \mathrm{CH_2CO} \rightarrow \mathrm{CH_2Mu} + \mathrm{CO}\,.$$

There are considerable practical difficulties involved in using ketene, which tends to polymerize in addition to posing significant safety hazards. Accordingly, we started with the relatively benign ketene dimer, which is a liquid at room temperature. Also, since any ketene sample will slowly evolve into an equilibrium mixture with its dimer, it was important to characterize the product of the reaction between Mu and diketene.

There are several potential sites for Mu addition in diketene (see structure 1 in Fig. 101). However, the transverse field μSR spectrum shows that only one product is formed. This is evident from the example in Fig. 102. The difference between the two radical precession frequencies (marked R_1 and R_2) is a direct measure of the muon hyperfine coupling constant (hfc). A different technique, muon avoided level-crossing spectroscopy, is used to determine proton hfcs. An example of such a μALCR spectrum is given in Fig. 103. The existence of two distinct resonances implies that the muoniated radical contains two sets of chemically inequivalent protons. A structure that satisfies these criteria is shown as 2 in Fig. 101. This assignment was supported by density functional calculations.

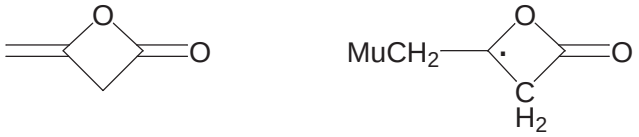

1 **2**

Fig. 101. The structure of (1) diketene; (2) the free radical formed by Mu addition to diketene.

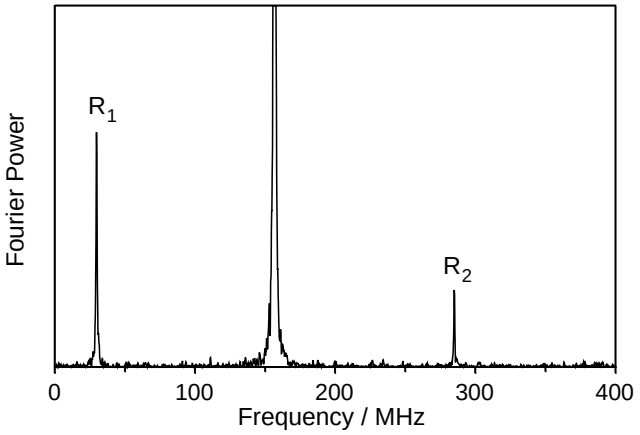

Fig. 102. Fourier transform μSR spectrum of the Mu adduct of diketene at 298 K and 11.6 kG.

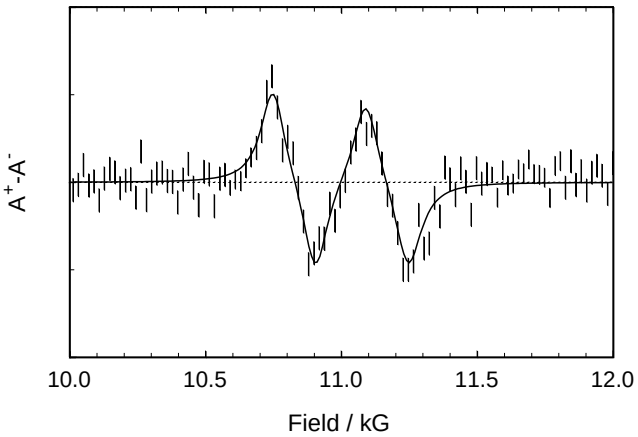

Fig. 103. μALCR spectrum of the Mu adduct of diketene at 298 K.

Muon and proton hfcs were determined at several temperatures between 280 and 363 K. The results are summarized in Table IX. The temperature dependence was modelled by taking into account the relative energies of the minimum energy conformations for rotation of the CH_2Mu group. Further details can be found in our publication [McKenzie *et al.*, Phys. Chem. Comm. **27**, 1 (2001)].

Table IX. Analysis of μALCR spectra.

T/K	A_μ/MHz	A_{p1}/MHz	A_{p2}/MHz
281.8	258.61	52.40(8)	46.62(8)
297.0	255.19	52.88(6)	46.56(5)
320.9	250.65	52.95(6)	46.21(5)
343.5	246.98	53.70(5)	46.56(6)
362.5	244.11	53.85(7)	46.60(7)

The next stage in the project was to use pure ketene as a sample. It was necessary to prepare fresh samples (by the pyrolysis of acetone) just prior to beam time, and store them in dry ice prior to mounting in a precooled cryostat. Our success is evident from the spectra shown in Figs. 104 and 105. The muon and proton hfcs

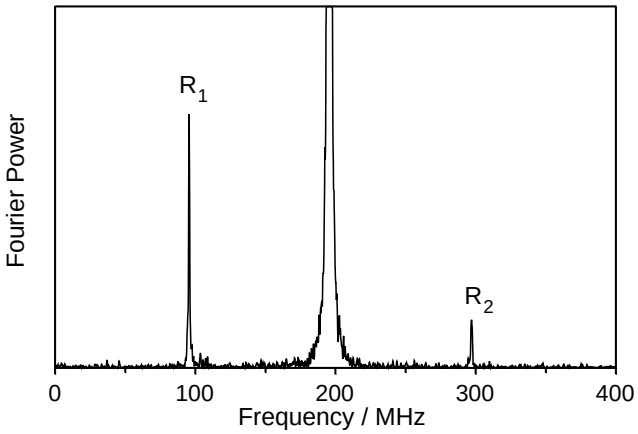

Fig. 104. Fourier transform μSR spectrum of the muoniated methyl radical at 184 K and 14.5 kG.

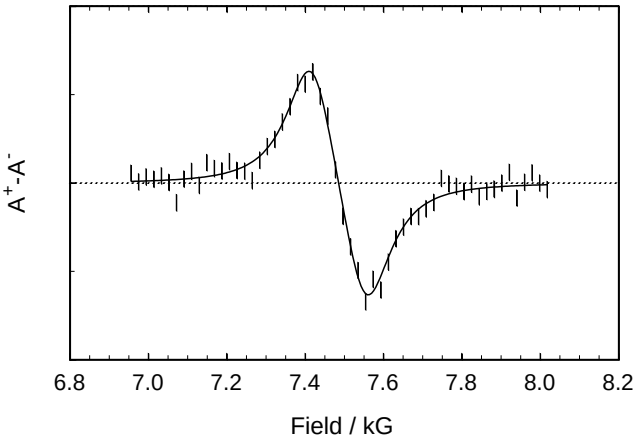

Fig. 105. μALCR spectrum of the muoniated methyl radical at 184 K.

were determined to be –201.5 MHz and –61.4 MHz, respectively. Since the ratio of these numbers differs by only a few per cent from that of the muon and proton magnetic moments, we can deduce that the Mu and H are chemically equivalent (with a small isotope effect of about 3%). There is little doubt that the radical is indeed the sought-after methyl, $\cdot CH_2Mu$.

Experiment 884
μSR studies on magnetic ground state of S=1/2 kagomé spin system $Cu_3V_2O_7(OH)_2\cdot 2H_2O$
(A. Fukaya and Y.J. Uemura, Columbia)

A copper volbothite $Cu_3V_2O_7(OH)_2\cdot 2H_2O$ is a system which has S=1/2 Cu moments on a nearly kagomé lattice configuration [Hiroi *et al.*, J. Phys. Soc. Jpn. **70**, 3377 (2001)]. Antiferromagnetic coupling is inferred from the Weiss temperature Θ = –115 K of the susceptibility at high temperatures. The spin dynamics of this system is of much interest in view of the interplay between the geometrical frustration and the enhanced quantum effect due to $S = 1/2$, as well as of the comparison with theories available for the $S = 1/2$ kagomé lattice antiferromagnet.

We performed ZF- and LF-μSR studies in the pure x=1.0 and diluted ($x \geq 0.6$) compounds. Figure 106 shows the temperature dependence of the time spectra at LF = 100 G in the pure system. The relaxation rate increased with decreasing temperature, indicating slowing down of Cu spin fluctuations, and then showed saturation below $T = 1.5$ K, as shown in Fig. 107. The LF dependence of the spectra at 50 mK was much smaller than that expected for static internal fields. These results, similar to the μSR results in $S = 3/2$ $SrGa_{12-x}Cr_xO_{19}$ kagomé magnets [Uemura *et al.*, Phys. Rev. Lett. **73**, 3306 (1994)], indicate slow dynamic spin fluctuations persisting to $T \to 0$.

The magnetic dilution resulted in a dramatic reduction of the relaxation rate, as shown in Fig. 107.

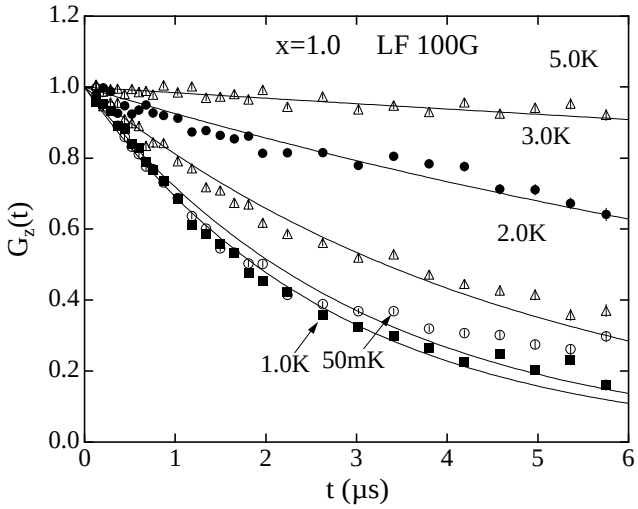

Fig. 106. Temperature dependence of the time spectra at LF = 100 G in the pure $x = 1.0$ sample.

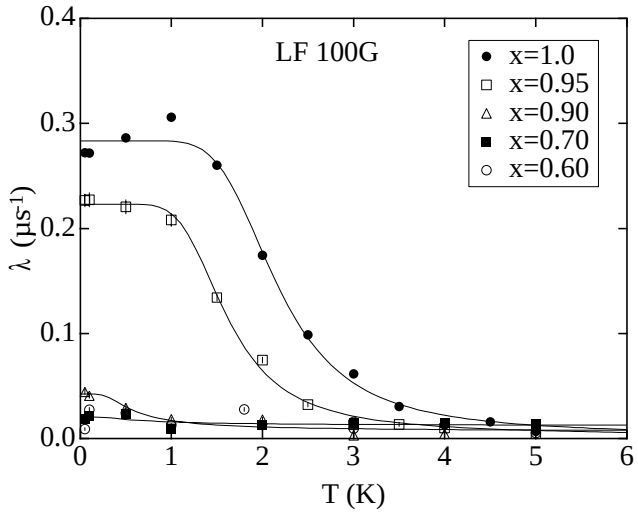

Fig. 107. Temperature dependence of the relaxation rate, λ, at LF = 100 G in various x samples.

This suggests that the observed relaxation in the pure system is not due to impurity spins. Instead, with increasing dilution (decreasing x), the spin fluctuation becomes faster.

Experiment 890
Anisotropic Kondo effect in $Ce_{0.8}La_{0.2}Al_3$?
(D.E. MacLaughlin, California, Riverside)

The theory of the anisotropic Kondo model (AKM) has been studied extensively in recent years. In spite of this interest there have been few experimental studies of physical realizations of the AKM in systems of local d or f moments in metals, which were the earliest manifestations of the "ordinary" Kondo effect.

The heavy-fermion compound $CeAl_3$ was long thought to exhibit a nonmagnetic "Kondo-lattice"

ground state. μSR and NMR studies showed, however, that inhomogeneous weak-moment magnetic order sets in below ∼1 K. Moreover, as lanthanum is doped onto cerium sites the specific heat coefficient $\gamma(T) = C(T)/T$ is drastically modified, and a maximum in $\gamma(T)$ at a characteristic temperature T^* ($\approx$ 0.4 K in $CeAl_3$) moves up in temperature and grows into a large peak; $T^* = 2.2$ K for $x = 0.2$. This behaviour was initially taken as evidence for development of a weak-moment magnetically ordered phase of $CeAl_3$, and attributed to reduction of the hybridization between Ce f electrons and ligand-derived conduction electrons.

This interpretation has been called into question on the basis of inelastic neutron scattering experiments on $Ce_{0.8}La_{0.2}Al_3$, which found a broad inelastic peak below T^*. This peak was taken as evidence for applicability of the AKM to the $Ce_{1-x}La_xAl_3$ system. Zero-field μ^+ spin relaxation (ZF-μSR) experiments at the ISIS pulsed muon facility indicated magnetic freezing at $T = T^*$, but the frozen moment was claimed to be weak (∼0.05 μ_B/Ce ion), principally because no neutron diffraction peak was observed. Recent ZF-μSR studies, also carried out at ISIS, conclude that for $x = 0.05$ the magnetic freezing persists to temperatures well above T^*. This is taken as further evidence that the specific peak at T^* reflects the anisotropic Kondo effect and is unrelated to spin freezing.

Specific heat measurements in $Ce_{0.8}La_{0.2}Al_3$ at applied fields of up to 14 T disagree with the theoretical behaviour of the AKM, however. Furthermore, the argument for applicability of the AKM depends strongly on evidence that the frozen moments are small, viz., the absence of neutron Bragg peaks. Neutron diffraction would not necessarily be sensitive to spin freezing of a glassy nature or short-range order, however, whereas the ZF-μSR relaxation rate reflects spin freezing independently of the degree of long-range order.

We have carried out ZF-μSR experiments in $Ce_{1-x}La_xAl_3$, $x = 0$ and 0.2, at TRIUMF and PSI. For $x = 0.2$ we observe a strongly damped but resolved oscillation in the muon asymmetry data at low temperatures, as shown in Fig. 108. For both La concentrations the precession frequency disappears at T^*, in disagreement with earlier results for $x = 0.05$, and in agreement with the expected result if T^* were a magnetic ordering transition temperature. The strong damping indicates a distribution of static local fields at muon sites, as might be expected in a strongly disordered substitutional alloy, but the oscillation reflects a fairly well-defined average local field. Asymmetry data for both La concentrations were fit assuming magnetic and nonmagnetic volume fractions; a "damped cosine" form was used for the precessing signal. The form of the relaxation function is

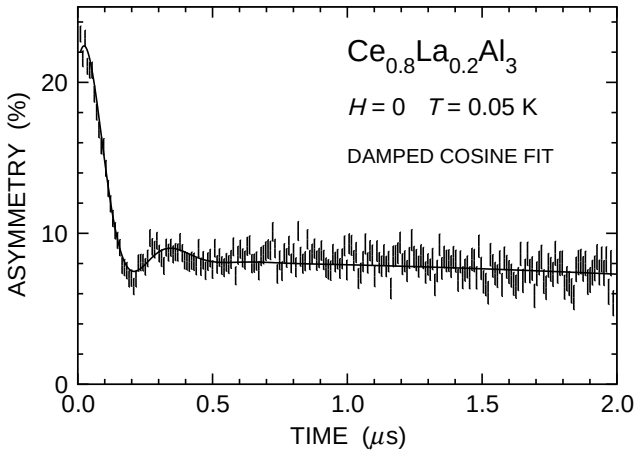

Fig. 108. $Ce_{0.8}La_{0.2}Al_3$ asymmetry relaxation function.

$$G(t) = A_m\left[\tfrac{2}{3}\exp(-\lambda_T t)\cos(2\pi\nu t+\phi) + \tfrac{1}{3}\exp(-\lambda_L t)\right] + A_n G_{\rm KT}(t)\,.$$

Here the relaxation from the magnetic volume fraction $f_{\rm mag}$ is modelled by the component with asymmetry amplitude A_m. The static field at the muon site is assumed to be randomly oriented. Relaxation of muons in the remaining nonmagnetic fraction is due to nuclear dipolar fields and is described by a static Kubo-Toyabe function $G_{\rm KT}(t)$; thus $f_{\rm mag} = A_m/(A_m + A_n)$. The relaxation rates λ_T and λ_L characterize the transverse and longitudinal relaxation, respectively; the former is expected to be dominated by static disorder whereas λ_L reflects dynamic spin-lattice relaxation.

The temperature dependence of the fit parameters is given in Fig. 109. It can be seen that $\nu(T)$ (a) is independent of x at low temperatures, (b) decreases markedly as T^* is approached from below, and (c) is suppressed to zero at $T = T^*$ for $x = 0.02$. Unfortunately the muon stopping site in $CeAl_3$ is not known, otherwise the ordered moment $\mu_{\rm ord}$ could be estimated accurately. Estimates of $\mu_{\rm ord}$ range from 0.11 to 0.5 μ_B/Ce ion in $CeAl_3$, which is 2–10 times larger than the neutron-diffraction upper limit reported previously, and the muon frequencies in $CeAl_3$ and $Ce_{0.8}La_{0.2}Al_3$ are the same. The entropy release at T^* implies $\mu_{\rm ord} \approx 0.3\ \mu_B$/Ce ion, comparable to values obtained from NMR and other measurements.

In $CeAl_3$, $\nu(T)$ is not completely suppressed to zero and $\lambda_T(T)$ increases rapidly at T^*; this can be understood as an effect of inhomogeneity in the transition temperature, as observed in La_2CuO_4. No such increase in broadening is observed in $Ce_{0.8}La_{0.2}Al_3$. $CeAl_3$ also exhibits a decrease of $f_{\rm mag}$ as T^* is approached from below; this is also not seen in $Ce_{0.8}La_{0.2}Al_3$.

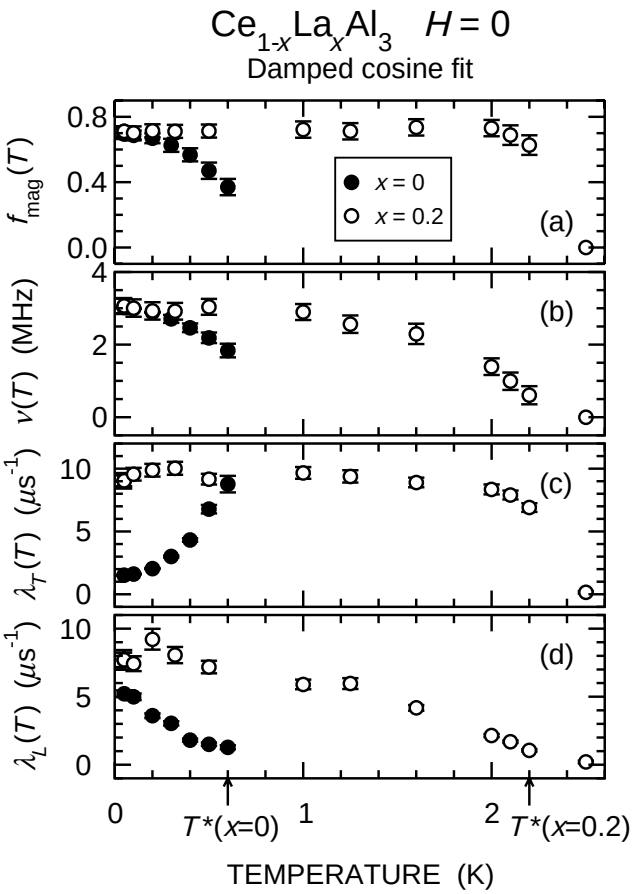

Fig. 109. Temperature dependence of (a) magnetic volume fraction $f_{\rm mag}(T)$, (b) precession frequency $\nu(T)$, (c) transverse relaxation rate $\lambda_T(T)$, and (d) longitudinal relaxation rate $\lambda_L(T)$ from ZF-μSR in $Ce_{1-x}La_xAl_3$, $x = 0$ and 0.2.

In conclusion, our ZF-μSR data are consistent with a scenario in which the specific heat anomaly in $Ce_{1-x}La_xA_3$ is associated with the onset of static magnetism below T^*, with or without long-range order. In particular, there is no sign of such static magnetism above this temperature in $Ce_{0.8}La_{0.2}Al_3$.

Experiment 891
Superconductivity and magnetism in $Ce_nT_mIn_{3n+2m}$
(G.D. Morris, LANL)

Introduction

Experiment 891 is investigating superconductivity and magnetism in the family of Ce-based heavy-fermion superconductors $Ce_nT_mIn_{3n+2m}$, T=Rh, Ir, Co. These materials share a common crystal structure made up of layers of $CeIn_3$ and TIn_2 stacked along the c axis. Their superconducting and magnetic properties vary widely with composition, so the set of materials provides a rich phase diagram (Fig. 110) for a systematic study. Of particular interest is the region of the

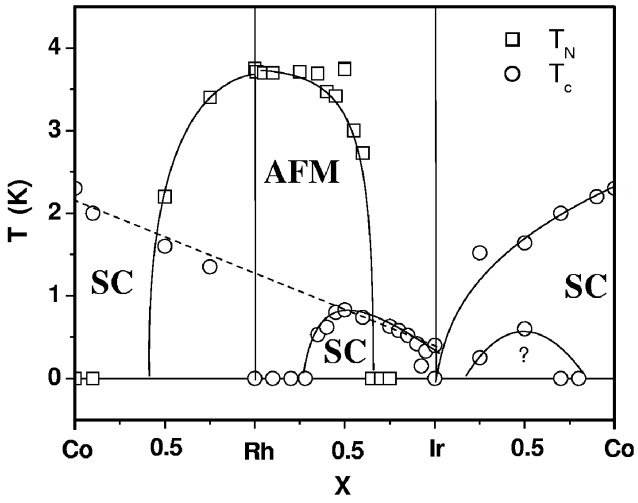

Fig. 110. A composition-temperature diagram of $CeTIn_5$ materials showing the superconducting (SC) and antiferromagnetic (AFM) phases [Pagliuso *et al.*, cond-mat/0107266].

phase diagram where superconductivity and AFM order coexist.

Muon spin relaxation experiments can provide unique information in several ways. The relative shift in muon precession frequency (Knight shift) probes the local spin susceptibility of electrons responsible for superconductivity. Linewidths reflect the magnetic field distribution, in principle enabling a determination of magnetic penetration depth in the superconducting state. In zero applied field the muon is a sensitive probe of internal fields generated by spontaneous magnetism.

$CeIrIn_5$

We performed a zero field experiment to search for spontaneous magnetism in a single crystal of $CeIrIn_5$. The experiment was carried out after quenching the superconducting solenoid of the dilution refrigerator and accurately zeroing the residual magnetic field to less than 20 mG. (Field zeroing was accomplished using the Mu signal in Si as a magnetometer because Mu has a gyromagnetic ratio 103 times larger than the muon.) The ZF muon spin relaxation (Fig. 111) was found to be well characterized by a static Gaussian Kubo-Toyabe function with a temperature-independent relaxation rate $\sigma_{\rm KT}$=0.239(4) μs^{-1} across T_c. No evidence for spontaneous magnetism in superconducting $CeIrIn_5$ was found.

$CeIr_{0.75}Rh_{0.25}In_5$

Substituting Ir with Rh in $CeIr_xRh_{1-x}In_5$ at first suppresses T_c, with a minimum at about $x = 0.93$. followed by a steady rise in T_c with the Rh fraction. $CeRhIr_5$ at ambient pressure is known from neutron scattering experiments to be an antiferromagnet with $T_N = 3.8$ K. This material has an incommensurate

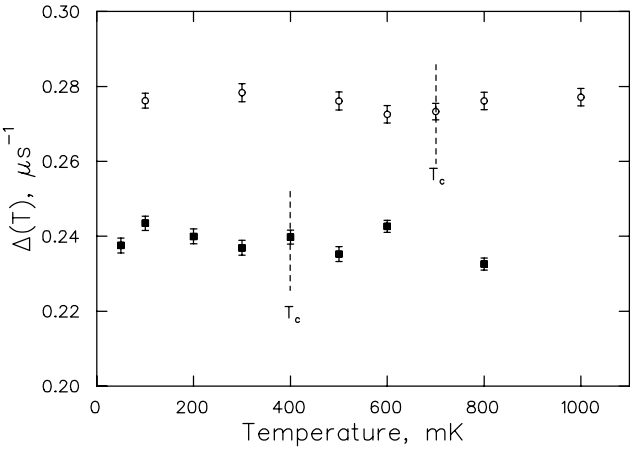

Fig. 111. Kubo-Toyabe relaxation rates $\Delta(T)$ in $CeIr_{0.75}Rh_{0.25}In_5$ (circles) and $CeIrIn_5$ (squares) show no significant change across their respective superconducting transition temperatures T_c.

magnetic order in which n-n Ce moments are antiferromagnetically aligned within the $a-b$ plane, but twist 107° per unit cell along the c axis. Muon spin relaxation experiments can probe the magnetism on a microscopic scale, and preliminary results indicate that the superconductivity and magnetic order coexist locally. This past summer we performed zero field measurements on the $x = 0.75$ composition, over a range of temperatures from 0.1 to 1 K to search for the development of local magnetic moments near T_c. The spin relaxation rate was found to be temperature-independent at $\sigma_{KT} = 0.276(2)\ \mu s^{-1}$ across T_c.

Status of Expt. 891

We plan to continue to survey a variety of the Ce-based HF materials, including n=2, m=2 materials, to study the relation between magnetism and superconductivity in this family of heavy fermion superconductors.

Experiment 894
Muonium kinetics and free radical formation in solutions of fullerenes

(B. Addison-Jones, UCC Kamloops)

The objective of this experiment is to obtain information on muonium substituted fullerenyl radicals in aqueous solution. This project evolved from previous results (Expts. 749 and 654) on such radicals in organic solvents. Experiment 894 was initiated in December, 2000 and approved for further beam time in June, 2001.

Aqueous solutions of fullerenes have long been sought for their application in biological systems. For example, it has been reported that substituted fullerenes inhibit HIV-1 protease activity. Due to the inherent hydrophobicity of fullerenes, these solutions were of low concentration or involved derivatizing the fullerene with a hydrophilic substituent. Recently, two new methods of producing aqueous fullerene solutions have been published, one involving the use of ultrasound and the other using redox reactions. Our group has tested both methods with the aim of producing solution concentrations high enough for detection of free radical signals and muonium decay rates. To date, concentrations of up to 100 μM have been prepared. These were characterized using UV absorption and dynamic light scattering, the latter with the cooperation of the SFU Physics Department. Aqueous fullerenes are thought to be colloidal in nature, with a range of cluster sizes. Dynamic light scattering provides the hydrodynamic radius of these particles in solution. Kinetics results from time-differential μSR measurements of muonium decay rates, together with application of diffusion controlled reaction theory, then allows us to determine the number of C_{60} molecules per cluster.

The original proposal aimed to study the kinetics of muonium addition to C_{60} by two methods, from muonium decay and from radical signal amplitudes in low magnetic field. If thermalized, Mu adds to a colloidal C_{60} particle consisting of N C_{60} molecules according to

$$\mathrm{Mu} + (\mathrm{C_{60}})_N \rightarrow (\mathrm{C_{60}})_N\mathrm{Mu}\,;$$

the first-order decay rate of muonium is given by $\lambda = k_{\mathrm{Mu}}[(\mathrm{C_{60}})_N]$ where k_{Mu} is the second-order rate constant for the reaction. Experimentally, the decay rate in pure solvent (λ_0) must be taken into account, to give

$$\lambda_{\mathrm{exp}} = \lambda_0 + k_{\mathrm{Mu}}[(\mathrm{C_{60}})_N]\,.$$

Note that since N was originally unknown, only $k'[\mathrm{C_{60}}]$ could be determined, where $k' = k_{\mathrm{Mu}}/N$. Muonium decay rates have been measured in 7–10 G with varying $[\mathrm{C_{60}}]$, yielding a rate constant of the order of 10^{10} $\mathrm{M^{-1}s^{-1}}$. The high value of the rate constant places this reaction in the diffusion controlled, as opposed to activation controlled, regime.

If the conventional Smoluchowski and Stokes-Einstein equations for diffusion controlled reactions apply to this reaction, the experimental rate constant should depend on the diffusion constants (D), radii (R), the Avogadro number (N_{Av}) and solvent viscosity (η) according to:

$$k = 4000\pi N_{\mathrm{Av}}(R_1 + R_2)(D_1 + D_2)$$

where

$$D = k_{\mathrm{B}}T/6\pi R\eta\,.$$

In this case, $R(C_{60N}) \gg R_{Mu}$ and $D_{Mu} \gg D(C_{60N})$, hence:

$$k = 4000\pi N_{Av} R(C_{60N}) D(Mu)\,.$$

$R(C_{60N})$ was measured by dynamic light scattering for a 3.67 μM colloidal sample, yielding a mean value of 100 ± 46 nm with no significant temperature dependence. The large variation in R is expected as C_{60} clusters, like many colloids, exist over a range of N values. Applying the above equations together with kinetics results then gave a mean cluster number of $N = 98 \pm 46$. This is in good agreement with published theoretical predictions based on molecular dynamics simulations.

To date, observations of radical signals from these colloidal C_{60} samples have been inconclusive. This may be due to product instability or additional mechanisms dephasing the Mu signal in the radical. Agreement of kinetic data based on the product, $(C_{60})_N Mu$, with that based on muonium decay is desirable as it provides direct evidence that the rate determining step in the reaction is indeed Mu + $(C_{60})_N$. However, new results for $^{12}C_{60}$ in an organic solvent, decalin, have been obtained. The use of an isotopically pure sample has eliminated extra splitting of the radical signals due to the presence of $^{13}C_{60}$. During reaction, loss of phase coherence between the precessing muonium spin and the muon spin in the radical reduces the signal intensity. The resulting radical polarization is given by:

$$P(\nu_{ij}) = \lambda^2/(\lambda^2 + \Delta_{ij}^2)$$

where Δ_{ij} depends upon the difference in precession frequency between muonium and the radical product. Selected μSR spectra for two representative fields are shown in Fig. 112. Results based on this method give a decay rate $\lambda = 2 \times 10^8$ s^{-1}, which is in accord with muonium decay results. However, the activation energy appears to be considerably higher than that obtained from muonium decay measurements. We continue to investigate whether it is indeed our mechanism or the application of conventional diffusion controlled reaction theory which needs modification in this case.

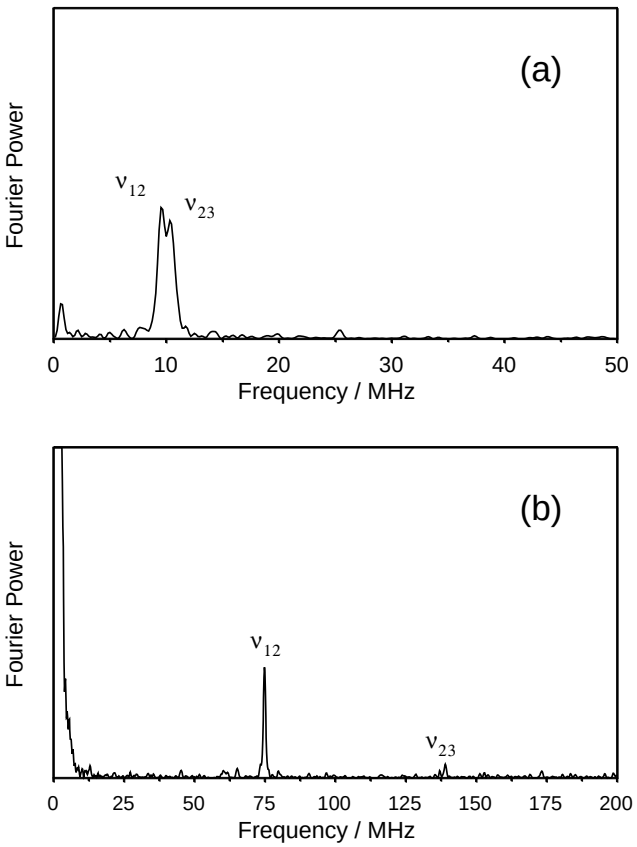

Fig. 112. Precession signals due to ν_{12} and ν_{23} in the radical $^{12}C_{60}Mu$ at (a) 7 G; (b) 77 G.

Experiment 912
Formation, structure, and dynamics of muonium in GaAs studied by EF-ALC-RF-μSR
(S.R. Kreitzman, TRIUMF; V.G. Storchak, Kurchatov; K.H. Chow, Alberta)

The goal of Expt. 912 is to improve the understanding of muonium formation, structure, and dynamics in certain bulk semiconductors by developing several new techniques to study such phenomena. These new methods are based on combining three, well-proven, powerful techniques: electric field EF-μSR, radio frequency RF-μSR, and avoided-level crossing (often called μLCR). Our plan was to initiate the experimental program by applying our new approaches to the technologically important semiconductor GaAs. On the one hand, these studies provide a "proof-of-principle" test of our new methods. At the same time, the results of these experiments dramatically enhance our understanding of the formation processes of light impurities in semiconductors. In this report, we briefly outline our preliminary progress in the development and application of these techniques.

The first of the two new techniques that we will describe combines EF with ALC. In semi-insulating GaAs at low temperatures, virtually no diamagnetic muonium is formed upon muon implantation. However, primarily from conventional transverse field measurements [Eshchenko *et al.*, Phys. Lett. **A264**, 226 (1999)], it is well established that by applying an electric field either along or in opposition to the incoming muon, one can increase the formation probability of diamagnetic muonium (with a concomitant decrease in the likelihood of forming to Mu^0_{BC}, the paramagnetic muonium state located near the centre of a Ga-As bond). However, no spectroscopic evidence exists regarding the site or the charge of the diamagnetic state,

although the most likely candidates are either isolated Mu^+ or Mu^-. Our goal with the EF-ALC technique was to obtain direct spectroscopic evidence which will allow us to elucidate the nature of this centre. Our plan was to enhance the diamagnetic signal by applying an electric field, and then compare it with the experimentally identified ALC signatures of isolated Mu^+ and Mu^- in heavily doped GaAs. As described in Expt. 791 in this Annual Report, for example, these two isolated states are easily distinguished since they give rise to ALC resonances that occur at very different magnetic fields. Our preliminary EF-ALC results are shown in Fig. 113. The existing data suggest the intriguing result that a resonance associated with Mu^+ (due to the nearest neighbour ^{71}Ga isotope) is seen in the direction of the electric field that we have labelled E+, while no such resonance is observed with the electric field in the opposite direction (E−). (The electric field is applied either parallel or anti-parallel to the incoming muon direction.) In other words, the data indicate that different charged states of muonium are formed depending on the direction of the electric field. In the upcoming beam period, our intention is to test if this conclusion is indeed correct by improving the signal-to-noise ratio of the signal, and to search for the signature resonances of Mu^- that exist at lower fields.

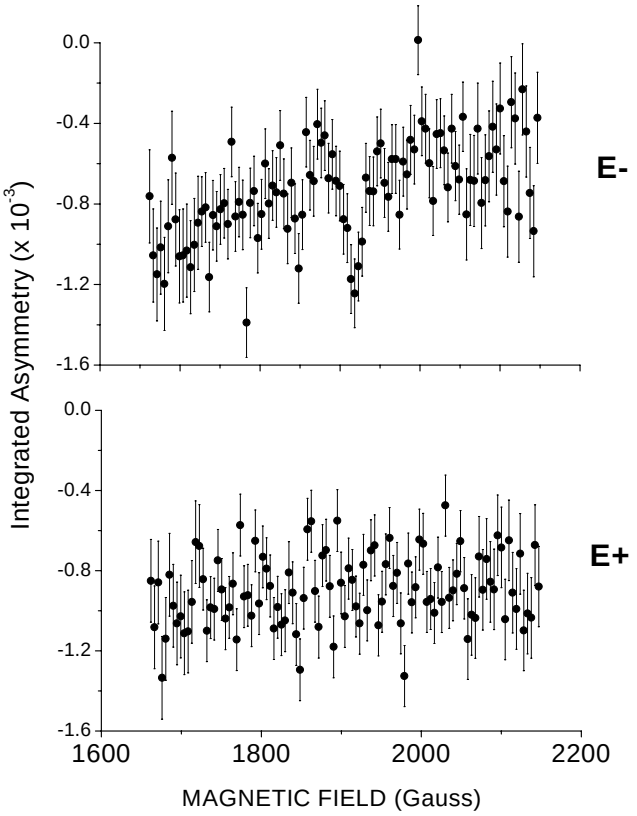

Fig. 113. EF-ALC spectra at 10 K in semi-insulating GaAs with $\mathbf{B}||\langle 100\rangle$.

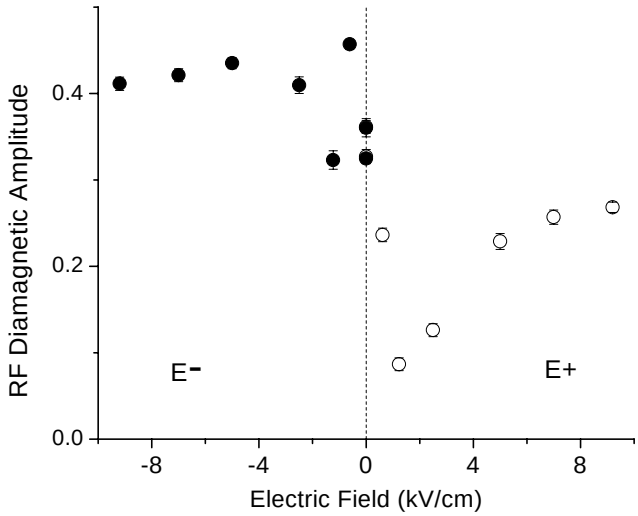

Fig. 114. EF-RF spectra at ≈50 K in semi-insulating GaAs with $\mathbf{B}||\langle 100\rangle$.

The second of the two new techniques is based on combining EF-μSR with RF-μSR. The electric field is used to modify the concentration of electrons around the muon and change initial muon/muonium fractions (as alluded to above), and RF-μSR is used to directly detect and study the dynamics of the final muonium/muon states that are formed. An example of the EF-RF data is shown in Fig. 114, which plots the electric field dependence of the diamagnetic amplitude in the E+ and E− directions. It is clear that we can detect an enhancement in the rf diamagnetic signal when the electric field is applied. At the same time, there appears to be a dramatic difference between the results in the electric field directions, especially at small values of E. This behaviour is unexpected and was not observed in the conventional TF-μSR studies. Further studies are clearly needed to understand the underlying mechanism responsible for formation of the final diamagnetic state(s).

In conclusion, our results, although preliminary, strongly suggest that the two new techniques will play an important role in future studies of muonium in semiconductors. Already, we have obtained fascinating science results using both new methods which we intend to pursue during the next beam period.

Experiment 915
Muonium in semiconductor alloys
(R.L. Lichti, Texas Tech)

Semiconductor alloys are being developed for specific applications, especially for heterojunction based devices, or for situations where a specific band gap is desired. Hydrogen is an important impurity in many semiconductors because of its chemical activity, especially its capacity to bond with other impurities to modify their electrical or optical activity. Experiment

915 continues our efforts to obtain detailed information on the behaviour of isolated H impurities by studying its light pseudo-isotope, muonium, which is far more accessible, experimentally. We chose to concentrate on the $Si_{1-x}Ge_x$ alloys during the initial week of beam time for this experiment, taken in mid-November. Our main goal was to determine how hyperfine constants for the two neutral muonium states, Mu^0_{BC} and Mu^0_T, vary across the alloy range. For instance, is there a single alloy-averaged hyperfine value or does the local mix of nearest neighbours yield distinct spectra? Based on motional properties this could be the case for Mu^0_{BC} but would not be expected for the mobile T-site species.

We examined three samples with $x = 0.2$, 0.5, and 0.77 to broadly span the full range. All spectra were with $\mathbf{B}\|[100]$; the four BC orientations are equivalent. Figure 115 shows hyperfine spectra at 3 T and roughly 70 K for the three samples. The displayed region includes the diamagnetic frequency, Mu^0_{BC} spectra, and the lower field Mu^0_T line. There are small shifts for the BC peaks and all lines are broader for the two higher Ge content samples compared with $x = 0.20$. The very broad Mu^0_T feature for the $x = 0.77$ sample, as well as the much sharper line for $x = 0.2$, are reproduced near 1400 MHz, confirming that these lines are from the isotropic Mu^0_T centre with a hyperfine value near 2000 MHz. No clear Mu^0_T spectra were observed for the 50/50 alloy.

In addition to the differences seen in the spectra at any particular temperature, the temperature dependences were significantly different for each sample, and apparently do not vary linearly between those of the elemental parent materials. We will need to perform a more careful time-domain analysis before the temperature variations seen in the Fourier spectra can be made quantitative. For the $x = 0.2$ sample we see low temperature growth of both neutrals at the expense of the diamagnetic signal up to above 50 K. The Mu^0_T signal amplitude peaks around 70 K followed by transfer from the T site into the BC site at least up to the BC ionization region between 160 and 200 K. For Si, the T to BC transfer occurs well above the BC ionization region which is around 140 K, while for Ge bi-directional site transfers occur below 100 K, while the onset of Mu^0 ionization is near 160 K; thus in many respects the $x = 0.2$ sample shows dynamics closer to those for the minority Ge component, while the hyperfine spectra are much more like those in Si.

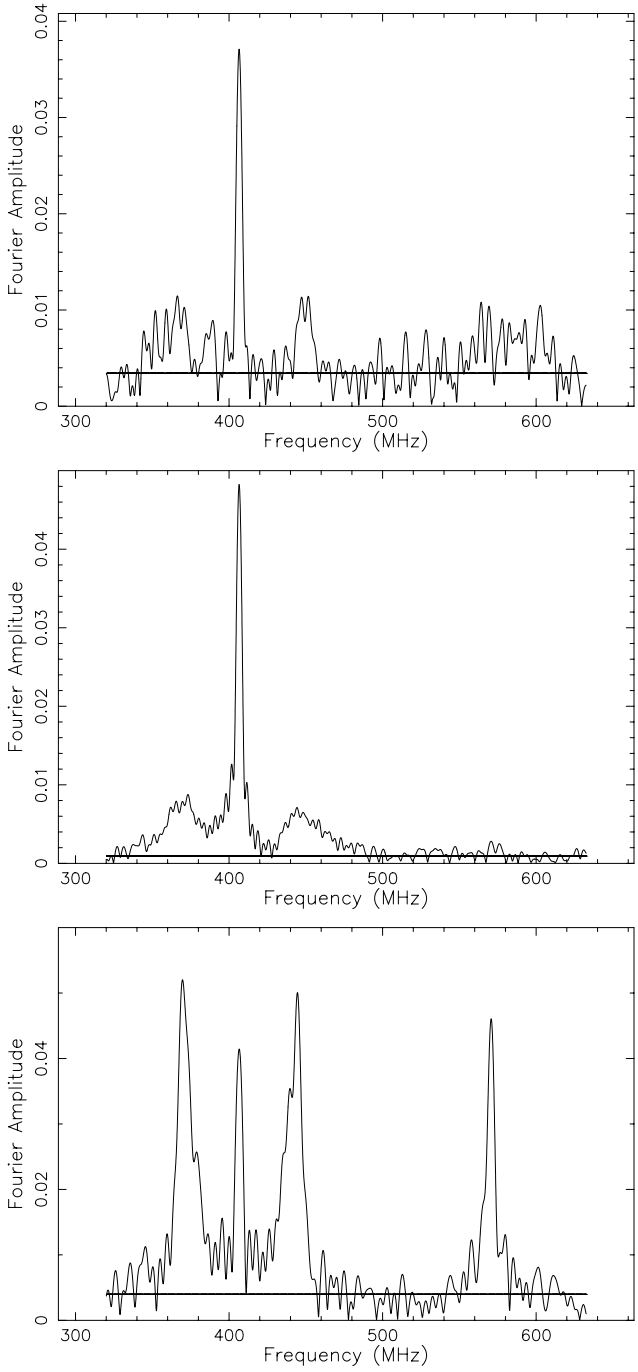

Fig. 115. Hyperfine spectra for three $Si_{1-x}Ge_x$ alloy samples: from bottom to top, $x = 0.20$, $x = 0.50$, and $x = 0.77$. Crystals were provided by I. Yonenaga, Tohoku University.

Experiment 916
QLCR of diamagnetic muonium states in GaP
(R.L. Lichti, Texas Tech)

Zero-field depolarization functions imply that there are several different diamagnetic muonium states present in doped GaP. TRIUMF Expt. 916 has as its main goal the identification of these different states us-

ing quadrupolar level-crossing resonances (QLCR) as our primary technique. The Ga isotopes produce two sets of nearly identical resonances at a field ratio of 1.59 giving a clear signature of Ga near neighbours to the muon location. Since P has no quadrupolar nuclei, any line not having such a partner must be related to an impurity atom. We started our investigation by examining an n-type sample near room temperature where the expected state is an isolated Mu^-. This state should be in the T_{Ga} interstitial location, based on theory and earlier results from GaAs [Chow *et al.*, Phys. Rev. **B51**, 14762 (1995)]. The spectra for a p-type GaP:Zn sample were also obtained at 670 K where the state should be a Mu-Zn pair based on zero-field results and analogy to results for GaAs:Zn.

Figure 116 displays part of the room temperature spectra for the n-type sample. Due to time constraints, we concentrated on a high statistics run to verify lines seen between 20 and 36 mT in an initial scan. Both data sets are shown in the figure; the line just below 30 mT is confirmed by the high statistics results but the two smaller lines within this region remain suspect. Additional data over a broader field region will be required to get structural data for the expected Mu_T^- state. Based on the single strong line seen thus far the field gradient is somewhat larger than for the same state in GaAs. The line at low field is probably from a Mu^+ state locally tunneling around a central P atom, since we expect a mix of Mu^+ and Mu^- in this $10^{16}cm^{-3}$ n-type sample. Any additional work on Mu^- will use more heavily doped material.

Figure 117 is the high temperature result for the Mu-Zn complex in heavily Zn-doped p-type GaP. These spectra are very similar to what we observed for this pair state in GaAs [Chow *et al.*, Phys. Rev. Lett. **87**, 216403 (2001)]. We speculated that this low field

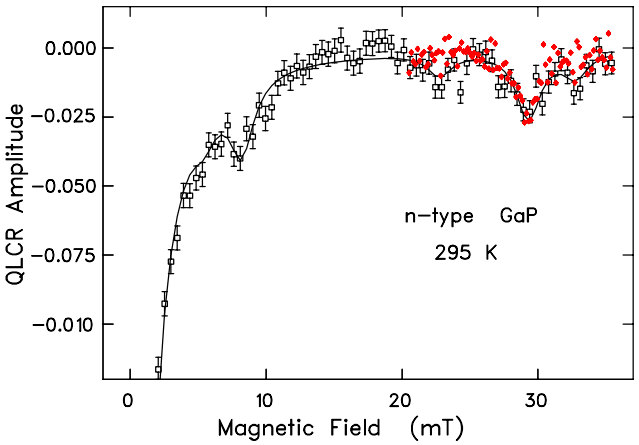

Fig. 116. Partial QLCR spectra for n-type GaP at room temperature. The filled points (red) are for a high statistics run, verifying a strong resonance at 29.5 mT: this should be part of a four line Mu_T^- spectra similar to GaAs results.

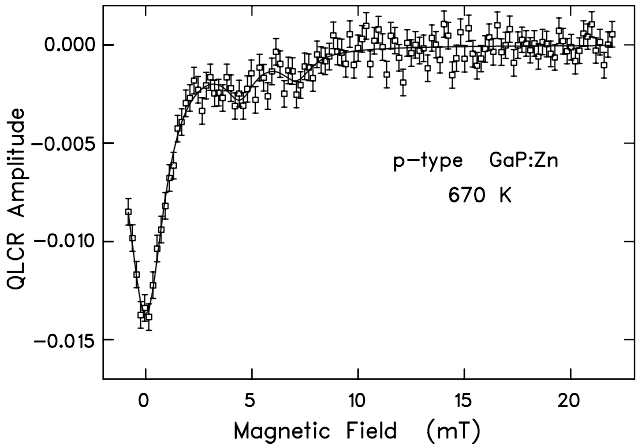

Fig. 117. The QLCR spectra for the Mu-Zn complex in p-type GaP:Zn shown here are nearly identical to the spectra for this complex at 530 K in GaAs, and imply a dynamic excited-state structural configuration.

feature is produced by Mu^+ local motion around the P (or As) near neighbour to the Zn impurity. This would be an excited state structure for the Mu-Zn pair rather than the Zn-Mu-P bond-centred ground-state configuration as expected for an acceptor-H complex. We note the similarity between the 670 K QLCR and the low field features in Fig. 116. If our state and structural assignments are correct, both of these cases (excited state structures of an isolated Mu^+ and of the Mu-Zn complex) involve local Mu^+ motion among the BC locations around a central P atom; thus they ought to yield very similar QLCR spectra, as observed.

Experiment 917
Correlation between magnetism and transport properties of thermoelectric oxides
(J. Sugiyama, Toyota Central R&D Labs; J.H. Brewer, UBC/TRIUMF)

Two cobalt oxides, $Ca_3Co_4O_9$ and Na_xCoO_2, were recently reported to exhibit metallic conductivities and extraordinary, large thermoelectric power coefficients (above +100 μV/K at 300 K), for reasons currently unknown. In order to investigate the role of magnetism on transport properties of such "good" thermoelectric oxides, muon spin rotation and relaxation (μSR) spectroscopy has been used for polycrystalline $Ca_3Co_4O_9$ and $Na_{0.7}CoO_2$ samples in the temperature range between 290 and 2.5 K. It was found that $Ca_3Co_4O_9$ exhibits a magnetic transition below $T_c^{\rm onset} \approx 100$ K with a transition width of $\Delta T_c = 70$ K. At temperatures below 100 K, two types of relaxation were observed using a weak transverse field μSR technique with $H = 104$ Oe; one exhibits a fast relaxation rate on the order of 10 μs^{-1} and the other a slow one of about 0.1 μs^{-1} (see Fig. 118). Furthermore, zero field μSR measurements suggested the existence of an

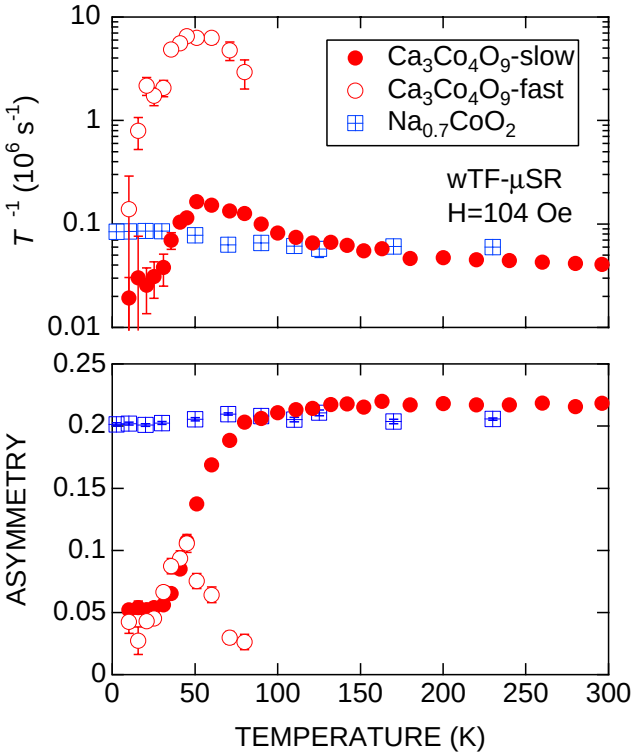

Fig. 118. Temperature dependence of relaxation rate and asymmetry of $Ca_3Co_4O_9$ and $Na_{0.7}CoO_2$.

incommensurate spin density wave state below $T_c^{\rm onset}$ (i.e. $T_c^{\rm onset} = T_{SDW}$).

This SDW transition was not detected by a dc susceptibility measurement, though a ferromagnetic transition was observed at 19 K in the χ vs. T curve. On the other hand, the resistivity vs. T curve exhibited a broad minimum around 80 K; in other words, $Ca_3Co_4O_9$ showed metallic behaviour above 80 K while semiconducting below 80 K. Therefore, the SDW transition was found to be associated with the change in the transport properties of $Ca_3Co_4O_9$.

The μSR studies on $Na_{0.7}CoO_2$ indicated no magnetic transitions around 100 K. Considering the difference of crystal structures between $Ca_3Co_4O_9$ and $Na_{0.7}CoO_2$, the Co ions in the rock salt-type layers of $Ca_3Co_4O_9$ were likely to play a dominant role to induce the SDW transition around 100 K.